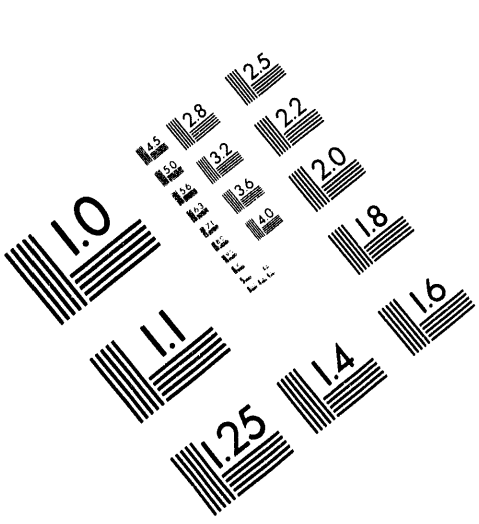

Association for Information and Image Management

1100 Wayne Avenue, Suite 1100
Silver Spring, Maryland 20910

301/587-8202

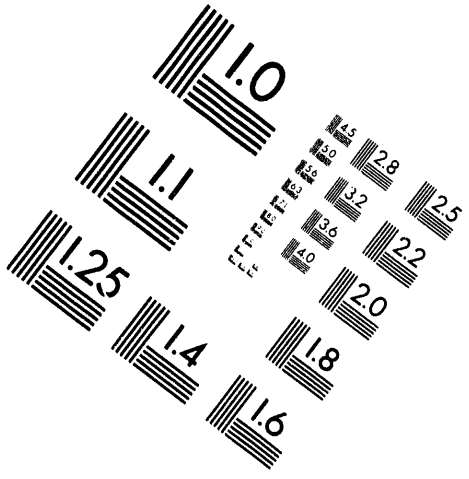

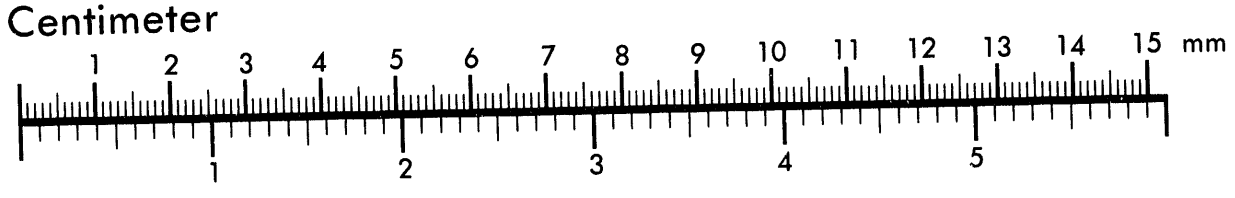

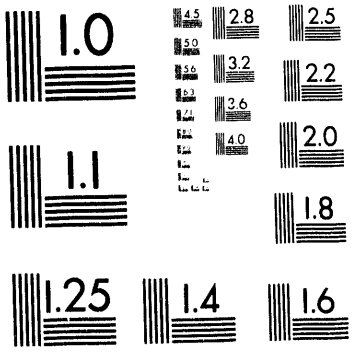

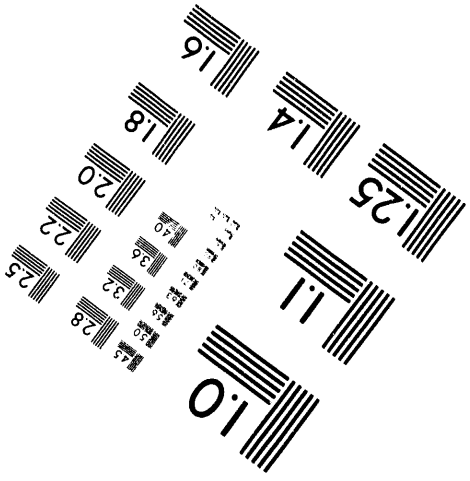

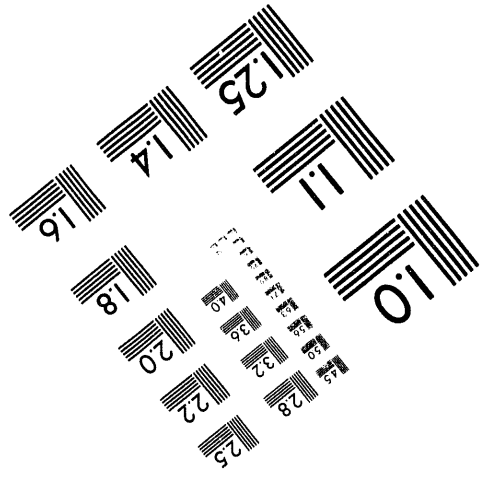

1 of 1

IS-T 1707

The Relationship of Structure to Superconductivity in the Pr-Ba-Cu-O System

by

Park, Minseo

MS Thesis submitted to Iowa State University

Ames Laboratory, U.S. DOE

Iowa State University

Ames, Iowa 50011

Date Transmitted: May 10, 1994

PREPARED FOR THE U.S. DEPARTMENT OF ENERGY

UNDER CONTRACT NO. W-7405-Eng-82.

DISCLAIMER

TABLE OF CONTENTS

ABSTRACT

The relationship of structure to the lack of superconductivity in the Pr-Ba-Cu-O system was systematically investigated. First, the phase equilibria of this system was studied to find the processing parameters which maximize the cation-site ordering between the Pr and Ba ions. Second, a comparative study between superconducting Nd-Ba-Cu-O and non-superconducting Pr-Ba-Cu-O was performed by forming solid-solution Nd-Pr-Ba-Cu-O.

Phase equilibria in the Pr-Ba-Cu-O system under varied oxygen partial pressures (PO_2) are investigated. It is found that stoichiometric $Pr_1Ba_2Cu_3O_{7-\delta}$(Pr123) does not exist when processed in air. Instead, nominal Pr123 is a mixture of $Pr_{1+x}Ba_{2-x}Cu_3O_{7+\delta}$ solid-solution ($Pr123_{ss}$) and $BaCuO_2$. As the PO_2 is lowered, the occupancy of the Pr ions on the Ba sites is decreased. The optimum oxygen pressure for ordering the cation-sites is found to be 0.01 to 0.001 atm. Further reducing the PO_2 causes other second phases to form. $Pr123_{ss}$ has a high antiferromagnetic ordering temperature ($T_N = 18.5K$).

The relationship between structure and superconductivity in $Nd_{1-x}Pr_xBa_2Cu_3O_{7-\delta}$ is investigated. A novel processing route is used to improve the homogeneity of the sample. Sharp superconducting transition temperatures (T_c) are achieved through this method. T_c decreases monotonically with increasing x and superconductivity disappears at around $x = 0.3$-0.4, which agrees well with data from other groups. It is found that Tc is enhanced by approximately 10K when the sample is processed at an oxygen partial pressure (PO_2) of 0.01 atm, followed by oxygenation at 450°C. Lattice constants of the sample are determined by Rietveld refinement of X-ray diffraction data. The depression of T_c as a

function of x and PO_2 is explained in terms of a charge-transfer model. It is suggested that destruction of superconductivity in the $RE_{1-x}Pr_xBa_2Cu_3O_{7-\delta}$ (RE=rare-earth) system can be viewed as the disruption of four-fold planar coordinated Cu ions in the chain-site due to the permanent occupation of extra Pr ions on the Ba sites.

GENERAL INTRODUCTION

In 1908, H. Kamerlingh Onnes discovered that the resistivity of mercury became vanishingly small bellow 4.2K [1]. This phenomenon is known as superconductivity. A superconductor is a material which shows zero electrical resistivity below a critical transition temperature (T_c). A thermodynamic phase transition from the superconducting to normal phase occurs at this temperature. Superconductivity is quenched when a critical magnetic field strength (H_c) or critical current density (J_c) in the sample is exceeded. Much research has been performed to find a material which exhibits superconductivity at higher temperatures. In 1986, Bednorz and Muller of IMB's Zurich Research Laboratory discovered a La-Ba-Cu-O ceramic superconductor whose T_c is 30K [2]. This achievement galvanized the attention of the international scientific community. Wu and Chu have discovered a Y-Ba-Cu-O superconductor which can be operated at 90K [3]. This discovery is significant since liquid nitrogen can be used to cool the sample instead of liquid helium which is expensive to use.

RE123 superconductors ($REBa_2Cu_3O_{7-\delta}$) have an oxygen-deficient perovskite structure, as shown in Fig. 1. The unit cell is composed of three layers of perovskite cells. The rare-earth ion is located in the center of the unit cell. Ba ions reside in the first and third layers of perovskite cells. Cu ions are located on the corners of each layers of perovskite. The Cu sites located in the basal plane are called Cu(1) sites, and the Cu sites on the second copper-oxide layer are referred to as Cu(2) sites. The second copper-oxide layer is frequently called the CuO_2 conduction plane since electrical conduction is believed

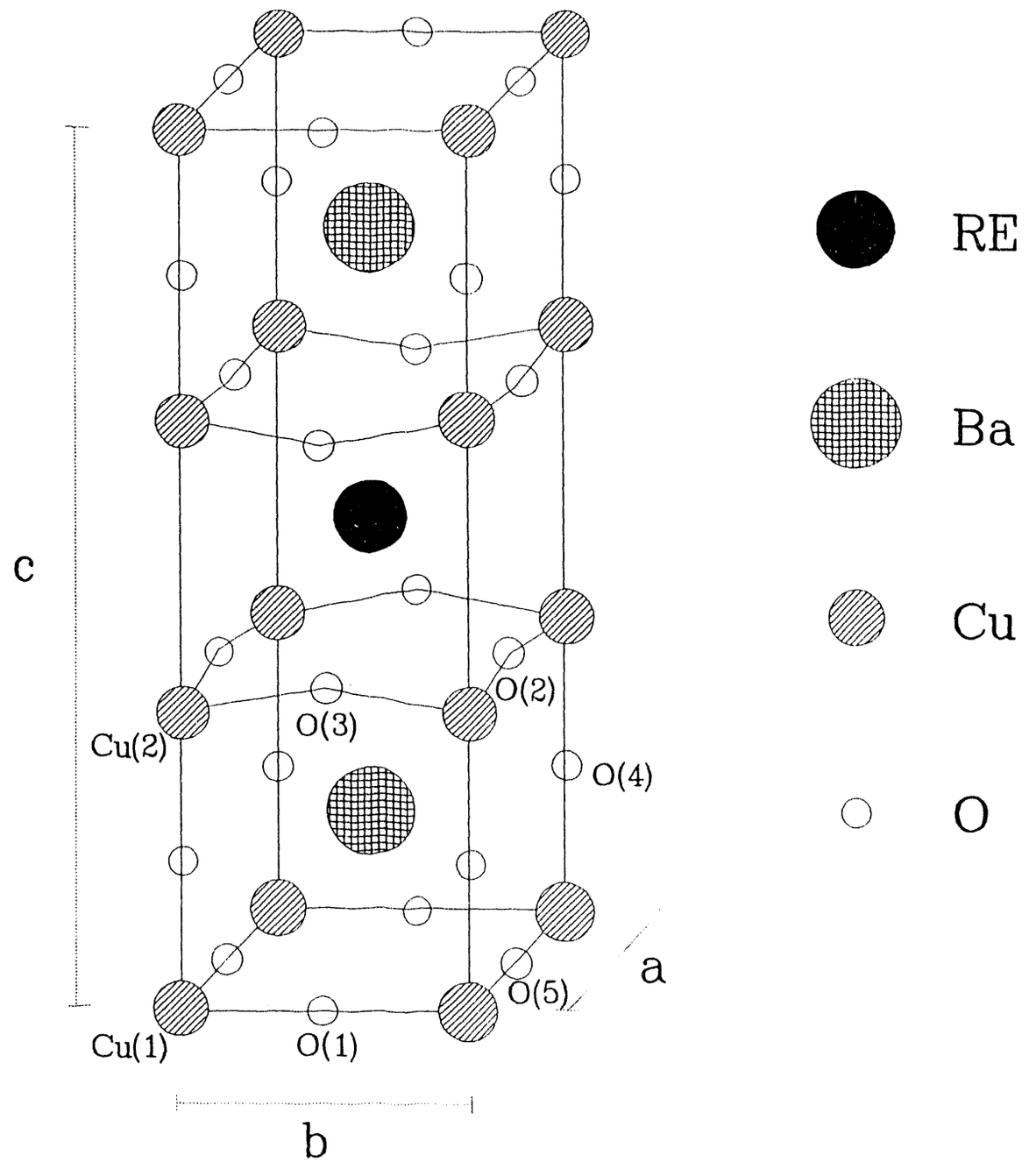

Figure 1 Crystal structure of RE-Ba-Cu-O

to be confined to this plane. The positions of the oxygen sites are as follows; O(1):[0 1/2 0], O(2):[1/2 0 z], O(3):[0 1/2 z], O(4):[0 0 z], and O(5):[1/2 0 0]. Among these, the O(5) sites are usually empty. RE123 superconductors are known as p-type superconductors, which indicates that the charge carriers are holes not electrons. Holes are created in the CuO_2 plane when electrons are transferred to the basal plane. Superconduction occurs two dimensionally along the CuO_2 conduction plane, while the basal plane plays a role of charge reservoir, transferring charge to the conduction plane. Oxygen doping occurs in the basal plane to create charge carriers in the conduction plane. The region of Cu-O(1)-Cu-O(1)-Cu ... in the basal plane are called chain sites, while Cu-O(5)-Cu-O(5)-Cu ... are referred to as anti-chain sites. The variation in oxygen content in the basal plane changes the oxidation state of the Cu ions in the chain sites. Slight changes in the oxygen content lead to charge transfer between the two planes.

A non-superconducting tetragonal structure with $\delta > 0.6$ is stable above about 700°C, and a superconducting orthorhombic structure with $\delta < 0.6$ is stable in air below that temperature. An ordered orthorhombic 'Ortho-1' structure (T_c=90K) with all occupied chain site is found when the value of δ is between 0 and 0.4, while ordered orthorhombic 'Ortho-2' phase (T_c=60K) with chain oxygen in every other chain site exists when $0.4 < \delta < 0.6$. The tetragonal structure can be formed from the orthorhombic structure by disordering the oxygen and vacancy located in the basal plane. This material undergoes an order-disorder phase transition. The low-temperature orthorhombic phase is formed below approximately 700°C due to oxygen ordering. The high-temperature tetragonal phase which has randomly distributed oxygen can be obtained by quenching the material from above 700°C to room temperature. The tetragonal RE123 structure is known to be semiconducting. The oxygen content in the RE123 system plays a critical role in determining superconducting properties; i.e., the higher the oxygen content, the higher

the transition temperature. This material should be fully oxygenated if a high quality sample is to be produced. The total oxygen content decreases as the temperature increases. Only those oxygen atoms which are located on the O(1) and O(5) sites can be removed from the structure. The O(5) sites are increasingly occupied by oxygen atoms with increasing temperature, while the total oxygen content is diminished. The abrupt structural change from the orthorhombic to tetragonal structure occurs when equal numbers of oxygen atoms occupy both O(1) and O(5) sites. Further increase in temperature causes the removal of oxygen from both of these sites. As the oxygen content decreases, the distances Ba-O(1), Ba-O(4), and Cu(2)-O(4) increase, while the distances Ba-O(2) and Ba-O(3) decrease [4].

The length of the orthorhombic lattice parameters a and b are so similar that they are frequently interchanged during the processing or tetragonal-to-orthorhombic phase transition. This kind of phenomenon is referred to as twinning. Twinning occurs to relieve the strain energy produced by the transition. Twin boundaries are believed to be flux pinning sites, where effective pinning can increase the critical current density. Effective flux pinning can be attained if the separation of pinning sites is on the order of one to five coherence lengths, where coherence length is the size of the Cooper-pair.

All rare-earth elements except Ce, Pr, Pm, and Tb, have been substituted for yttrium in $YBa_2Cu_3O_{7-\delta}$ (Y123) without destroying superconductivity (T_c=90K) [5-7]. Among these four exceptional elements, it is known that the Ce and Tb do not form a stoichiometric 123 phase [8]. The Pm compound has not been synthesized since the Pm nucleus is radioactively unstable [9]. $PrBa_2Cu_3O_{7-\delta}$ (Pr123) is, however, isostructural to other $REBa_2Cu_3O_{7-\delta}$ (RE123) systems, and yet it is neither metallic nor superconducting

[10]. Instead, Pr123 is an antiferromagnetic semiconductor with $T_N = 17K$ [11-16]. Why, then, is the $PrBa_2Cu_3O_{7-\delta}$ not conducting and therefore not superconducting?

Two qualitative models have been proposed to explain the absence of superconductivity in the Pr123 system [17]. The first idea is that hole-filling in the conduction band occurs due to the fact that the valence state of the Pr ions is higher than +3, resulting in a decrease in the number of holes. However, Electron Energy Loss Spectroscopy (EELS) measurements show that the total hole concentration does not change with increasing x in the $Y_{1-x}Pr_xBa_2Cu_3O_{7-\delta}$ system [18]. The other model suggests a hybridization of the praseodymium f-states with oxygen p-orbitals. This model, however, cannot explain the existence of superconductivity in the $Pr_{0.5}Ca_{0.5}Ba_2Cu_3O_{7-\delta}$ epitaxtial thin films [19].

From a structural point of view, it was considered that orthorhombic symmetry is essential for materials to exhibit superconductivity. However, tetragonal $CaBaLaCu_3O_{7-\delta}$ shows superconductivity with $T_c = 80K$ [20]. On the other hand, orthorhombic $NdBa_2Cu_3O_{7-\delta}$ which is crystallized from the amorphous state is found to be non-superconducting [21]. This is possibly due to the fact that the cation-sites are highly disordered. Jorgensen et al. [22,23] proposed that the structural coherence of the CuO_2 planes is the determining factor for superconductivity. They argued that this structural coherency can be achieved only if there is orthorhombic symmetry on at least a short length scale.

Calculations from Gupta and Gupta using first principle [51], and from Veal with empirical data [52] showed that four-fold planar coordinated (FFPC) Cu in the chain-site is the essential feature for superconductivity. Random occupation of the RE ions on the Ba site disrupt FFPC Cu, diminishing the number of available charge carriers in the conduction plane. Since the occupation of Pr ions on the Ba sites is more effective in

destroying superconductivity than the occupation of Nd ions on the Ba sites, we suggest that one of the possible reasons for why the Pr-Ba-Cu-O system is not superconducting is the destruction of FFPC Cu due to the random occupation of the Pr ions on the Ba sites. However, other effects cannot be disregarded.

The goal of this research is to investigate if the stoichiometric, perfect Pr123 phase can be formed, and if not, how far the nominal Pr123 structure deviates from the perfect 123 structure. We will also discuss how we can relate the cation site-disorder to the lack of superconductivity in the Pr123 system.

The research questions which were addressed during this investigation are as follows;

1) Is it possible to make a stoichiometric Pr123 by any means?

The attempt to prepare a stoichiometric Pr123 resulted in the production of the impurity phase of $BaCuO_2$ [26], and it was found there is an inconsistency in the phase-diagram among available literature [27].

2) How far does the nominal Pr123 deviate from the perfect 123 structure?

The crystal structure of the $Y_{1-x}Pr_xBa_2Cu_3O_7$ was studied by neutron diffraction as a function of x [28]. It is revealed that the normally vacant O(5) sites become occupied by oxygen with increasing x. The O(5) site occupancy might imply the presence of Pr ions on the Ba sites. The occupation of the trivalent rare-earth ions on the divalent Ba sites induces oxygen take-up to occur to satisfy the charge neutrality.

3) What is the lower solubility limit and phase stability under different O_2 partial pressures?

Subsolidus phase relationships at 950°C in the Pr-Ba-Cu-O system were studied by Hodorowicz et al. [27] According to their phase diagram, $Pr_{1+x}Ba_{2-x}Cu_3O_y$ ($-0.1 < x < 0.55$) solid solution occurs along the '123'-'336' tie line. They also mentioned that the Pr211 phase could not be synthesized.

4) What will happen to the phase diagram, crystal structure, and physical properties as we substitute Pr for Nd in Nd123?

The $Nd_{1-x}Pr_xBa_2Cu_3O_{7-\delta}$ system has been investigated by several groups [29-31]. The superconducting transition temperature T_c decreases monotonically with increasing x, and superconductivity disappears at around $x=0.3$. There is a slight disagreement on the actual shape of the T_c depression curve, although the general trend is the same. This is possibly due to the difference in the processing conditions or slight differences in oxygen content. The Nd-Ba-Cu-O system is especially interesting since the size of the Nd and Pr ions are similar and they are neighboring elements in the periodic table. Therefore, we can eliminate the effects due to the size difference of these ions.

The first part of this thesis is devoted to the phase equilibria study of Pr-Ba-Cu-O. To find a method to minimize the occupancy of the Pr ions on the Ba sites, phase equilibria as a function of the oxygen partial pressure was studied. The second part is a comparative study between superconducting $NdBa_2Cu_3O_{7-\delta}$ and non-superconducting $PrBa_2Cu_3O_{7-\delta}$. In order to understand the differences between these two systems, a structure-superconductivity relationship was studied by forming $Nd_{1-x}Pr_xBa_2Cu_3O_{7-\delta}$ solid solution.

EXPERIMENTAL PROCEDURE

Processing

Sample preparation in general

Before mixing, Nd_2O_3, Pr_6O_{11}, $BaCO_3$, and CuO powders were thoroughly dried in a muffle furnace. Nd_2O_3 and $BaCO_3$ were dried at 1000°C and 750°C for 24 hrs respectively. Pr_6O_{11} was dried at 900°C for 24 hrs and at 400°C for 24 hrs to insure the formation of stoichiometric Pr_6O_{11}. Binary Pr-O system has numerous derivative compounds due to the variety in the valence of the Pr ions. In order to fully oxidize CuO, it was dried at 550°C for 5 days. The powders were micromilled in a motorized mortar and pestle to obtain fine powders whose particle size is less than 10 μm. Fine-sized particles must be used in order to maximize the surface area, since the surface area of the particles in contact has an enormous influence on the reaction rate; i.e. the smaller the particle is, the higher the reaction rate. After weighing, they were mixed using a micromilling machine. Weighing and mixing were performed under an N_2 atmosphere to prevent the formation of paste due to the moisture picked up in air. The powders were pressed into pellets in order to further increase the contact area between particles and to reduce the initial porosity. The pellets were calcined in flowing CO_2-free, dry air at 890°C. The air flowing rate was 10 *l*/min. Differential thermal analysis (DTA) was used for the study of phase purity. This procedure was repeated until $BaCO_3$ was completely reacted.

After calcination, the powders were pressed into pellets to be sintered at 950°C in zero-grade oxygen with a flowing-rate of 50 cc/min. During sintering, densification occurs. The driving force for densification is a lowering in surface energy due to the reduction in the solid-vapor interface. There are three major events that occur at this stage; grain growth, change in pore shape, and reduction of pores. If a liquid phase is formed due to partial melting, grain growth will be accelerated. The liquid will wet the surface of the grain to lower the surface energy and it will pull two grains together due to the surface tension. Furthermore, transport of matter will be facilitated by the formation of liquid, followed by rapid grain growth [32]. In the RE-Ba-Cu-O system, our goal is to limit the formation of liquid since the existence of liquid can cause macroscopic compositional inhomogeneity and exaggerated grain growth. If the size of the grain is above 1 μm, microcracking may occur due to the high anisotropy in thermal expansion [33], especially at the tetragonal to orthorhombic phase transition. These cracks can be superconducting weak links.

Sample preparation for the study of phase equilibria

In order to investigate an isothermal section of the Pr(O)-Ba(O)-Cu(O) system at 880°C, powders with appropriate stoichiometry were pressed into pellets and sintered at 880°C in air. The temperature was held for 48 hrs to 5 days, depending on the reaction kinetics of the sample. The pellets were air-quenched to room-temperature by removing the sample from the furnace. In the study of the phase diagram of $Pr_{1+x}Ba_{2-x}Cu_3O_{7+\delta}$ as a function of the oxygen partial pressure, a specially designed furnace was used to cool the sample in an identical atmosphere. Fig. 2 shows a design of the furnace for this purpose. The opening of the slide chamber is completely sealed by an O-ring in order to preserve the atmosphere inside the furnace during the movement of the position of the sample. By

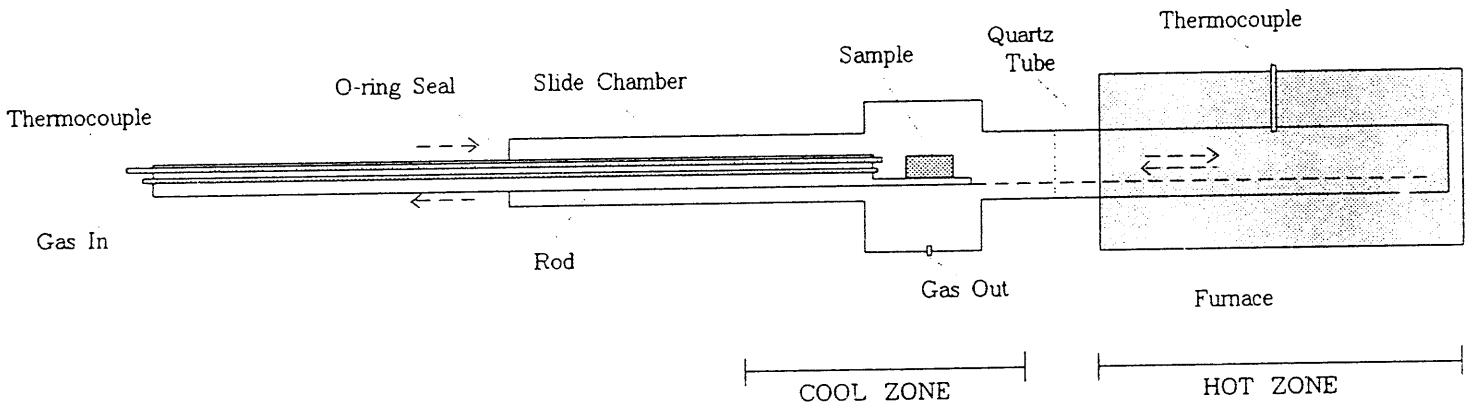

Figure 2 Design of the furnace which was used in this experiment

using this furnace the sample can be quenched inside the furnace without being pulled out to the air. Due to the difference in the atmosphere between the inside and outside of the furnace, removing the sample from the furnace might produce faulty results. After heat-treatment, the samples were quenched to room-temperature. Some of the samples were oxygenated at 450°C in an oxygen atmosphere.

Special technique to minimize RE occupation on the Ba site

Structural properties of the RE-Ba-Cu-O system are a strong function of their oxygen content and valence state. For the ions which have a large ionic radii (Nd,Pr,La, etc.), there is a tendency for the RE ions to form a solid solution.

$$(RE^{3+})[(Ba^{2+})_{2-x}(RE^{3+})_x](Cu^{2+})_2(Cu^{3+})(O^{2-})_7$$

Charge imbalance due to the occupation of trivalent RE ions on the divalent Ba sites is compensated by reduction of the Cu valence and oxygen uptake. Therefore, if we process the material under a low PO_2, we can prevent the RE ions from occupying the Ba sites. In order to order the cation sites (RE and Ba), the samples were heat-treated at a low PO_2. After the heat-treatment, the sample was quenched to room temperature in an identical atmosphere. Sintered pellets should be annealed at 450°C under O_2 in order to be further oxygenated. This procedure has nothing to do with the arrangement of the cations in the lattice, because the temperature is low enough not to move heavy cations like RE, Ba, etc. Only light elements such as oxygen can diffuse into the structure. During this process, the material will have an orthorhombic structure with space group Pmmm.

Special route to preparation of Nd-Pr-Ba-Cu-O solid solution

Due to the low melting temperature (T_m=970°C) of $PrBa_2Cu_3O_{7+\delta}$ and the possibility of producing unfavorable phases by invariant reactions, it is necessary to lower

the synthesis temperature of Pr123. Since the melting temperature of Nd123 is fairly high (1108°C) compared to that of Pr123, it is difficult to achieve complete solid-solubility in this system at low processing temperatures. As is shown in Fig. 5, both the Nd123 and Pr123 phase diagrams contain RE_2CuO_4 as a point compound, and it was confirmed that these compounds exhibit complete solid solubility with each other. Both Pr_2CuO_4 and Nd_2CuO_4 are isostructural and have a fairly high decomposition temperature (1250°C in air). Since $(Nd_{1-x}Pr_x)_2CuO_4$ solid solution has been successfully synthesized, these materials were used as precursors in order to enhance the homogeneity of the samples.

As a precursor material, $(Nd_{1-x}Pr_x)_2CuO_4$ (where x=0.1, 0.2, 0.3, 0.4, 0.5) was synthesized at 1100°C in air by mixing thoroughly dried Nd_2O_3, Pr_6O_{11}, and CuO powders. The heat-treatment was repeated until XRD and DTA confirmed the formation of a single phase solid-solution. $NdPr123_{ss}$ was prepared by mixing and heating appropriate amounts of $(Nd_{1-x}Pr_x)_2CuO_4$ (NdPr201), $BaCO_3$, and CuO powders at 880°C in air twice, then the heating temperature was raised to 950°C. After it was confirmed that $BaCO_3$ was fully reacted, they were heat-treated at 990°C in oxygen in order to increase the reaction kinetics. At this stage, the samples contained mostly $(Nd_{1-x}Pr_x)_{1+y}Ba_{2-y}Cu_3O_{7+\delta}$ solid solution and a small amount of $BaCuO_2$. In order to minimize the occupancy of Nd and Pr ions on the Ba sites, the samples were heat-treated at 0.01 atm oxygen partial pressure, followed by quenching. For comparison, samples which had the same composition were heat-treated at 1 atm PO_2 at 1000°C. The samples were oxygenated at 450°C in flowing oxygen to produce an orthorhombic structure.

Characterization

DTA (differential thermal analysis)

Thermal analysis was conducted with a Perkin-Elmer DTA 1700. The temperature of the sample was compared with that of high-purity alumina powder. The sample powder was weighed ≈ 40 mg and loaded in an alumina crucible. The composition of the gases was controlled by a Sierra gas flow controller. The DTA furnace was purged for 30 min before running in order to change the atmosphere completely. The gas flow rate was 50 cc/min. The heating rate of the DTA furnace was set at 10°C/min. The endothermic onset temperature was determined at the intersection point between the steepest tangent to the peak and selected base line. After the sample was cooled, it was studied by an X-ray diffractometer.

XRD (X-ray diffraction)

X-ray diffraction was conducted by a Philips diffractometor equipped with a vertical 2-theta goniometer and a Cu K_α radiator. The sample powder was sprinkled on top of a glass slide with a scratched surface and tapped with minimum pressure in order to prevent preferred orientation of the grains. Typical scanning rates were 0.05° per step from 20° to 70°. Each step was a 3 second period. Lattice constants were calculated using the FINAX and GSAS program software from XRD data. Silicon powder was used as an internal standard. In this case, a slow scanning rate, 0.02°(in 2Θ)/10sec from 15° to 85°, with a large number of data points was used. In order to minimize background noise, the pellet surface was diffracted by X-rays. For Rietveld refinement analysis the sample powders were ground and sieved to a particle size of less than 25 μm. In order to increase

the precision of the data collection, X-ray diffraction was performed by Dr. Victor G. Young Jr. using a Sintag XDS-2000 diffractometor. The X-ray powder pattern was refined by GSAS program software [34]. Rietveld refinement was done until a best-fit was attained between the calculated powder pattern and observed powder pattern.

SEM-EDS (scanning electron microscopy-energy dispersive spectroscopy) and Optical Microscopy

The microstructure of the sample was analyzed by a scanning electron microscope and optical microscope. The sample was cut into appropriately sized pieces and mounted in silver epoxy. After mounting, the surface of the sample was polished. A Cambridge S-200 SEM with EDS system was used for microstructural and compositional analysis of the sample. Backscattered electrons (BSE) and Secondary electrons (SE) were used as an imaging source. Accelerating voltage and working distance were 15 KV and 18 mm, respectively. X-ray spectra from the sample were collected by a Norton EDS system and relative amounts of the elements in the sample were semi-quantitatively analyzed.

SQUID (superconducting quantum interference device) Measurement

Superconductors exhibit perfect diamagnetism, and magnetic flux is completely expelled from the sample. If the temperature is raised above T_c, magnetic flux starts to penetrate the sample. The magnetic induction inside the material is described by

$$B = H + 4\pi M = (1 + 4\pi M X) H$$

where H is the external magnetic field strength, M is the magnetization, and X is the magnetic susceptibility. Below T_c, B=0

$$M = - H/4\pi$$

Since X = M/H, the susceptibility is

$$X = -1/4\pi$$

i.e. the material is diamagnetic.

Superconductor can be classified as Type-1 and Type-2. Type-1 material exclude all of an applied field to exhibit superconductivity. Rare-earth oxide superconducting material is known as type-2 superconductor, which means superconductivity remains over a range even after magnetic field penetrate the sample. This is different from type-1 superconductor where superconductivity is destroyed as soon as critical magnetic field is exceeded. The normal region which can be penetrated by flux is called fluxoid. The motion of fluxoid should be pinned by structural imperfections if critical current density is to be increased. The magnetization curves of type-2 superconductor is described in Fig. 3.

If the sample is cooled in the absence of the field, the diamagnetism after applying a field means exclusion of the magnetic flux from the sample. It should be noted that even though only a surface of the sample shows superconductivity, zero-field-cooled moment exhibit complete flux exclusion from the whole sample. In the mean while, when the sample is cooled with field, field-cooled (FC) susceptibility which is smaller than zero-cooled (ZFC) susceptibility is observed. This field-cooled moment represents true Meissner effect. Field-cooled susceptibility is significantly smaller than zero-field-cooled susceptibility. One of the plausible reason for this incomplete flux expulsion is flux pinning. The temperature where FC and ZFC magnetization curve meet each other is called irreversibility temperature T_{irr}. If pinning does not exist, FC and ZFC data should be identical. Hysteresis in magnetization curve is observed when the direction of applied magnetic field is reversed.

Magnetic and superconducting properties of the sample were studied by a Quantum Design MPMS SQUID magnetometer. Both field-cooled and zero-field-cooled magnetization curves and hysteresis loop data were collected. The magnetic Tc were

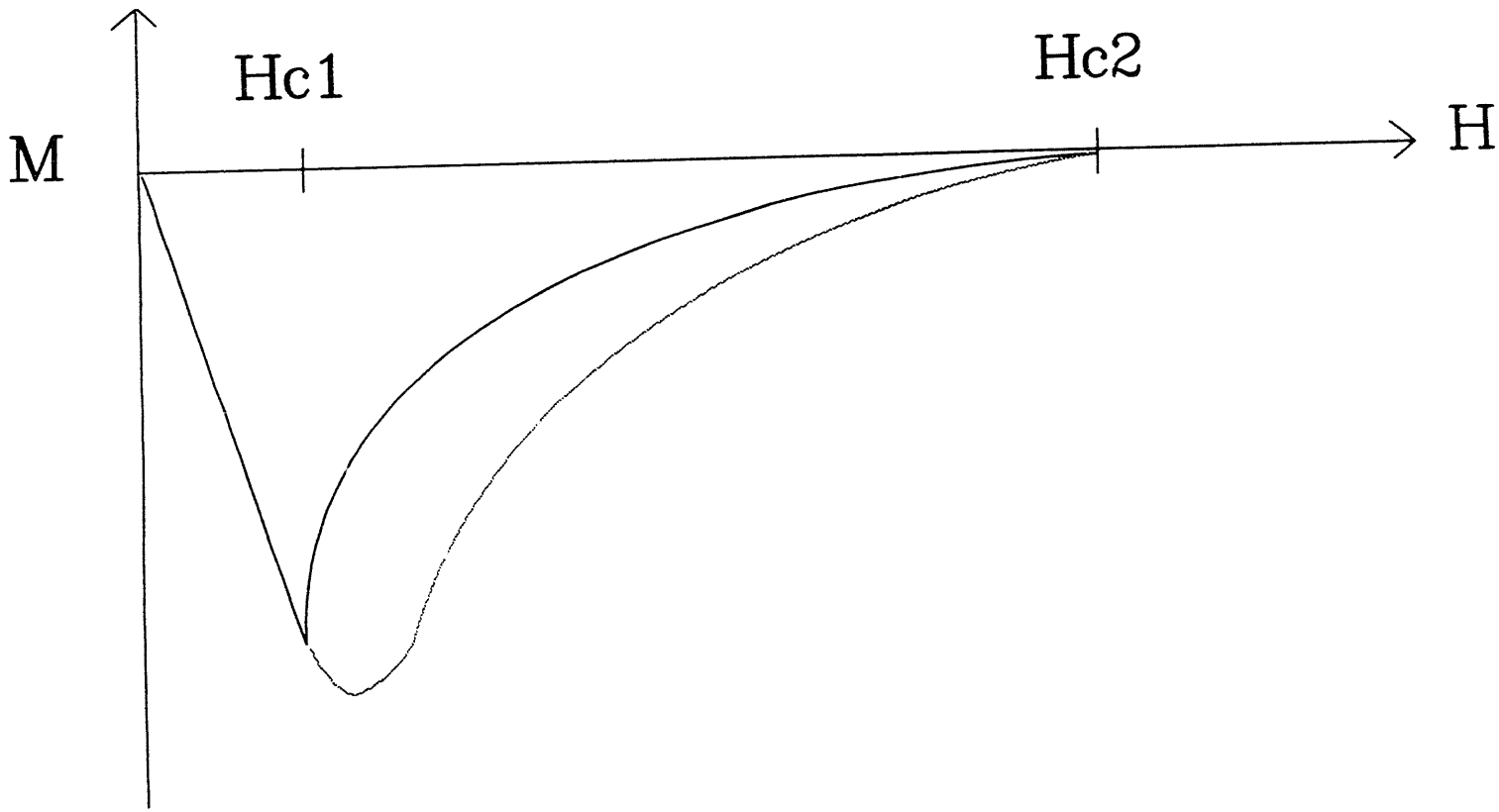

Figure 3 Magnetization curves of the type-2 superconductors
(Dotted curve represents a magnetization when a flux pinning exists.)

determined from these data. The diamagnetic moment of the superconducting samples was collected as follows; The sample was cooled from 150K to 5K without applying a field. At 5K, the diamagnetic moment was measured by increasing the applied magnetic field to 10 Oe. While the temperature of the sample was increased to 100K, the zero-cooled-field (ZFC) moment was measured in the 10 Oe magnetic field. After the sample was cooled to 5K , the field-cooled (FC) moment data was collected by increasing the temperature up to 150K. The Curie-Weiss behavior of the material was studied using a program which is programmed to collect values of magnetic moment with increasing applied magnetic field at each temperature (T=8, 10, 12, ..., 36K). A best fitted linear function M=f(H) was obtained using a linear regression method. The slope of this function was used as the magnetic susceptibility X at each temperature. A X^{-1} vs T graph was plotted and the types of magnetism were identified from that graph, since this kind plot is easy way to compare various kind of magnetism. Experimental confirmation of various kinds of magnetism in materials can be summarized in Fig. 4.

ICP-AES (Inductively Coupled Plasma Atomic Emission Spectroscopy) and Oxygen Content Determination

The cation ratios of the samples were analyzed by Inductively Coupled Plasma Atomic Emission Spectroscopy (ICP-AES). The oxygen contents of the samples were determined by an Inert Gas Fusion method. ICP-AES and Gas-fusion analysis were done at the Analytic Service Center in Ames Laboratory.

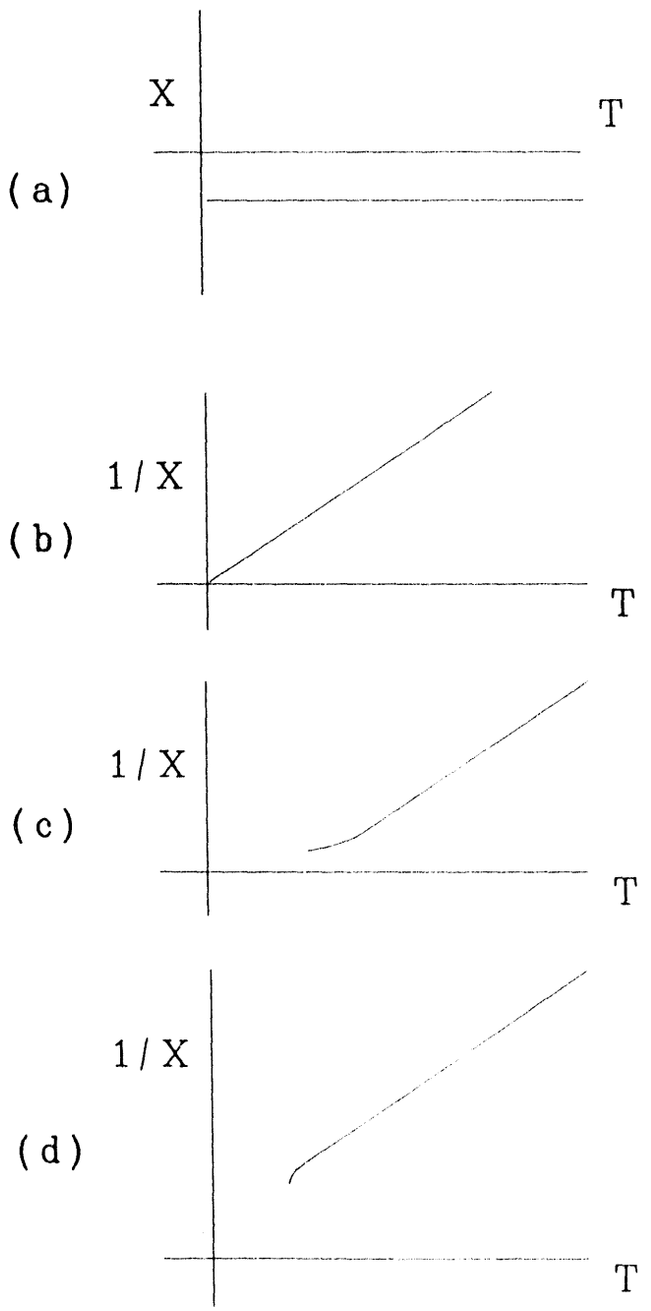

Figure 4 Experimental confirmation of the various kinds of magnetism (X is a susceptibility of the material) (a)diamagnetism (b)paramagnetism (c)ferromagnetism (d)antiferromagnetism

PART 1. PHASE EQUILIBRIA IN THE Pr-Ba-Cu-O SYSTEM UNDER VARIED OXYGEN PARTIAL PRESSURES

INTRODUCTION

Extensive research has been performed to investigate the puzzle of why Pr123 is not superconducting [11-16]. Most of the research in this area was concerned with the *Structure-Property* relationships of the materials, and it was assumed that Pr123 has perfect, stoichiometric 123 structure. However, growing evidence indicates that Pr123 does not have a perfect structure [26,35,36], and the structure of Pr123 can be varied significantly by employing different processing methods. In spite of this significance, little attention has been paid to the study of the *Processing-Structure* relationship in the Pr-Ba-Cu-O system. For example, the degree of the solid solubility between Pr^{3+} and Ba^{2+} ions can be varied by employing different processing parameters. In order to design the material to have a desired structure, an understanding of the phase equilibria is essential.

As can be seen in Fig. 5, there is a significant difference in the phase diagrams between Y-Ba-Cu-O and Nd(or Pr)-Ba-Cu-O due to the difference in ionic radii of rare-earth ions. Since the ions which have large ionic radii (Nd, Pr, La, etc) tend to form solid solutions with RE on the Ba sites, it is important to determine the solid solubility range in this system. Subsolidus phase relationships at 950°C in the Pr(O)-Ba(O)-Cu(O) system were studied by Hodorowicz et al. [27] According to their phase diagram, $Pr_{1+x}Ba_{2-x}Cu_3O_{7+\delta}$ ($-0.1 < x < 0.55$) solid solution occurs along the '123'-'336' tie line. This is inconsistent with the result of other authors who found that it is difficult to prepare single phase Pr123 [26,35,36]. To resolve this inconsistency, phase equilibria with emphasis on the Pr123 region and its vicinity was investigated. Some of the invariant reactions and the nature of these reactions were identified. In the Pr-Ba-Cu-O system, a knowledge of the

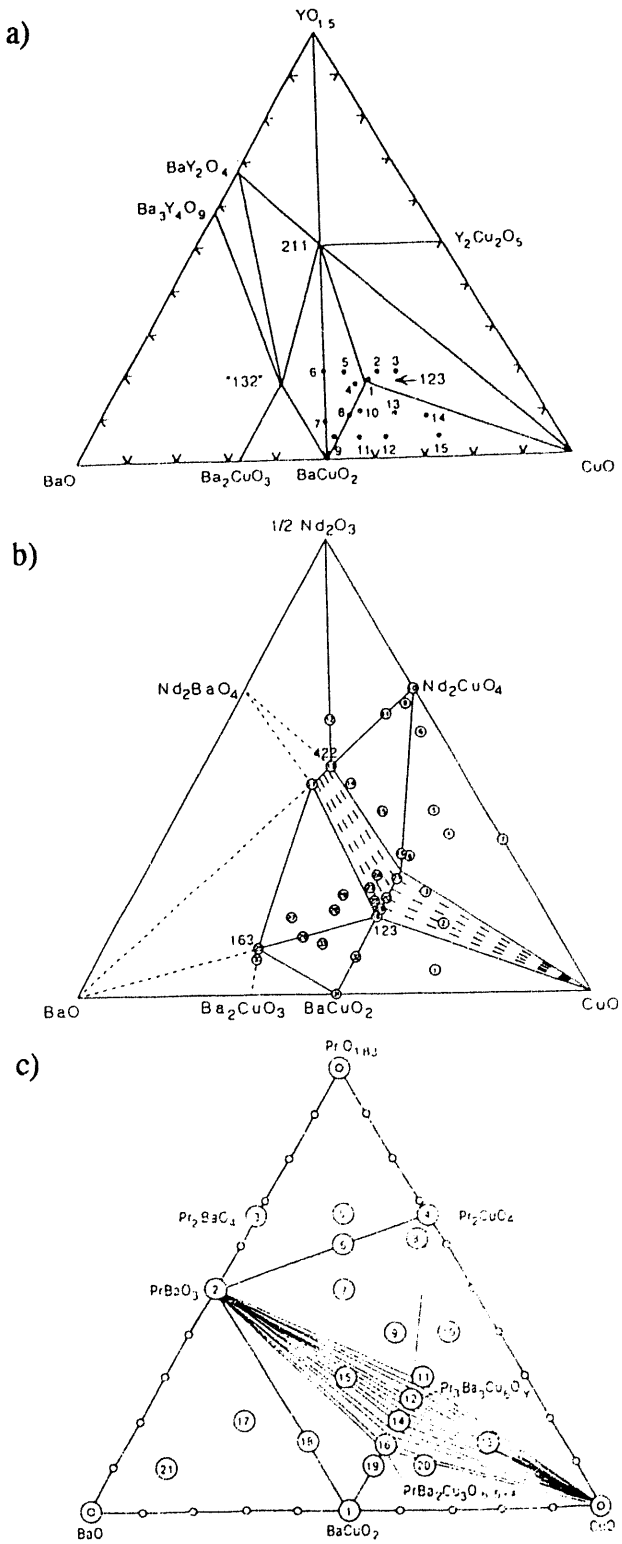

Figure 5 Phase diagrams of (a)Y-Ba-Cu-O, (b)Nd-Ba-Cu-O, and (c)Pr-Ba-Cu-O (From ref. 55, 56, 27, respectively)

degree of solid-solubility between the Pr and Ba ions as a function of the oxygen partial pressure is important because it is directly related to the purity of Pr123. In spite of this importance, no study has been done on this subject. Therefore, the phase diagram of $Pr_{1+x}Ba_{2-x}Cu_3O_{7+\delta}$ (x=0.0, 0.01, 0.02, 0.03, 0.04) as a function of the PO_2 (log PO_2= -2, -1, 0, 1, 2) was mapped out.

The major purpose of this research is to find the processing parameters which can minimize the occupancy of Pr ions on the Ba sites.

RESULTS AND DISCUSSION

Fig. 6 shows the phase diagram of the Pr(O)-Ba(O)-Cu(O) system at 880°C in air. The compositions of the samples and observed phases are summarized in Table 1. In general, the formation of liquid phases may cause additional difficulty in identifying phases. In order to avoid the formation of liquid the temperature was set to 880°C, since it has been found that the lowest melting event occurs at around 890°C in air in this system. The phase diagram of the $Pr_{1+x}Ba_{2-x}Cu_3O_{7+\delta}$ as a function of PO_2, and the observed phases, are shown in Fig. 7 and Table 2, respectively.

Isothermal section of the Pr(O)-Ba(O)-Cu(O) phase diagram at 880°C in air

The pseudo-binary system

The Ba(O)-Cu(O) system $BaCuO_2$ has been characterized by numerous investigators [37-39]. The crystal structure of $BaCuO_2$ as determined by electron diffraction is cubic with the space group {Im3m} [38]. It is known that $BaCuO_2$ melts in air between 1000°C and 1010°C [39].

The Pr(O)-Ba(O) system In an ambient oxygen atmosphere, a distorted perovskite type $PrBaO_3$ can be synthesized. Under a reducing atmosphere, Pr_2BaO_4 can be obtained [40]. Magnetic ordering in the $PrBaO_3$ compound has been studied via a neutron diffraction technique by N.Rosov. et al. [41] They argue that $PrBaO_3$ exhibits antiferromagnetic ordering below 11.7(2)K.

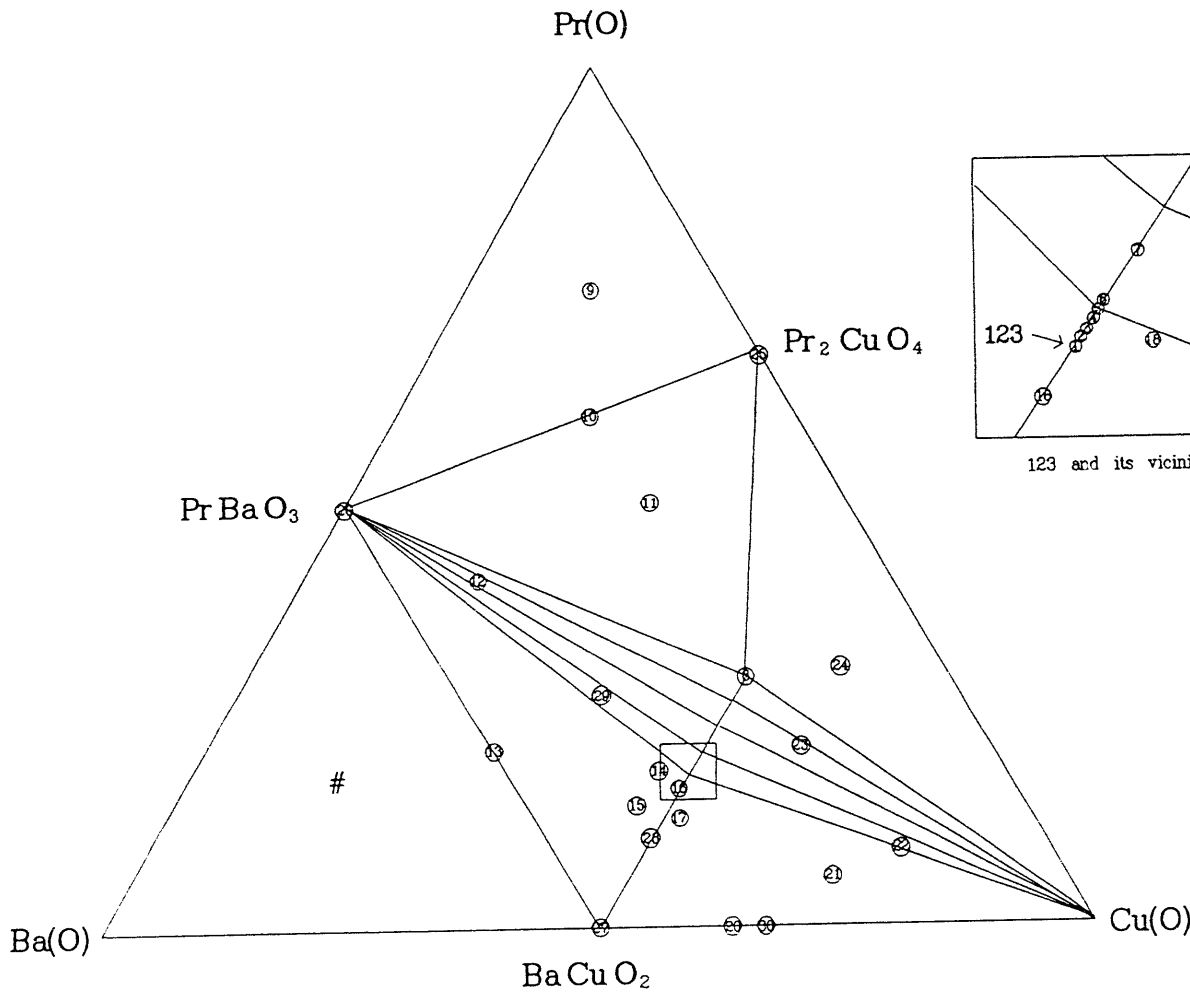

Figure 6 The isothermal section of the Pr(O)-Ba(O)-Cu(O) system at 880°C in air (#The Ba-rich region of the phase diagram was not studied.)

Table 1 Nominal compositions of the samples, and phases observed (from Fig. 6)

SAMPLE NUMBER	CATIONIC RATIOS Pr : Ba : Cu			PHASES OBSERVED
1	1.0	2.0	3.0	123_{ss}, 011
2	1.01	1.99	3.0	123_{ss}, 011
3	1.02	1.98	3.0	123_{ss}, 011
4	1.03	1.97	3.0	123_{ss}, 011
5	1.04	1.96	3.0	123_{ss}
6	1.05	1.95	3.0	123_{ss}
7	1.1	1.9	3.0	123_{ss}
8	1.7	1.3	3.0	123_{ss}^{+}
9	7.0	1.5	1.5	100, 110, 201
10	3.0	1.0	1.0	110, 201
11	5.0	2.0	3.0	123_{ss}^{+}, 110, 201
12	7.0	7.0	3.0	123_{ss}^{+}, 110
13	2.0	5.0	3.0	110, 011
14	4.0	8.0	11.0	123_{ss}, 110, 011
15	1.0	2.6	3.3	123_{ss}, 110, 011
16	7.7	16.3	24.0	123_{ss}, 011
17	1.0	3.0	4.2	123_{ss}, 011, 001
18	7.7	14.8	24.0	123_{ss}, 011, 001
19	8.8	15.2	26.0	123_{ss}, 001
20	0.0	3.0	5.0	011, 001
21	1.0	3.8	10.9	123_{ss}, 011, 001
22	1.0	1.7	8.3	123_{ss}, 001
23	1.0	1.0	3.0	123_{ss}^{+}, 001
24	3.0	1.0	6.0	123_{ss}^{+}, 201, 001
25	2.0	0.0	1.0	201
26	1.0	1.0	0.0	110
27	0.0	1.0	1.0	011
^28	1.0	3.7	4.7	
^29	1.0	1.4	1.4	
^30	0.0	1.0	2.0	

$123_{ss} = Pr_{1+x}Ba_{2-x}Cu_3O_{7+\delta} (x < 0.1)$

$123_{ss}^{+} = Pr_{1+x}Ba_{2-x}Cu_3O_{7+\delta} (x > 0.5)$

$011 = BaCuO_2$, $110 = PrBaO_3$, $201 = Pr_2CuO_4$, $100 = Pr_6O_{11}$, $001 = CuO$

^The sample of this comp. was studied only by DTA.

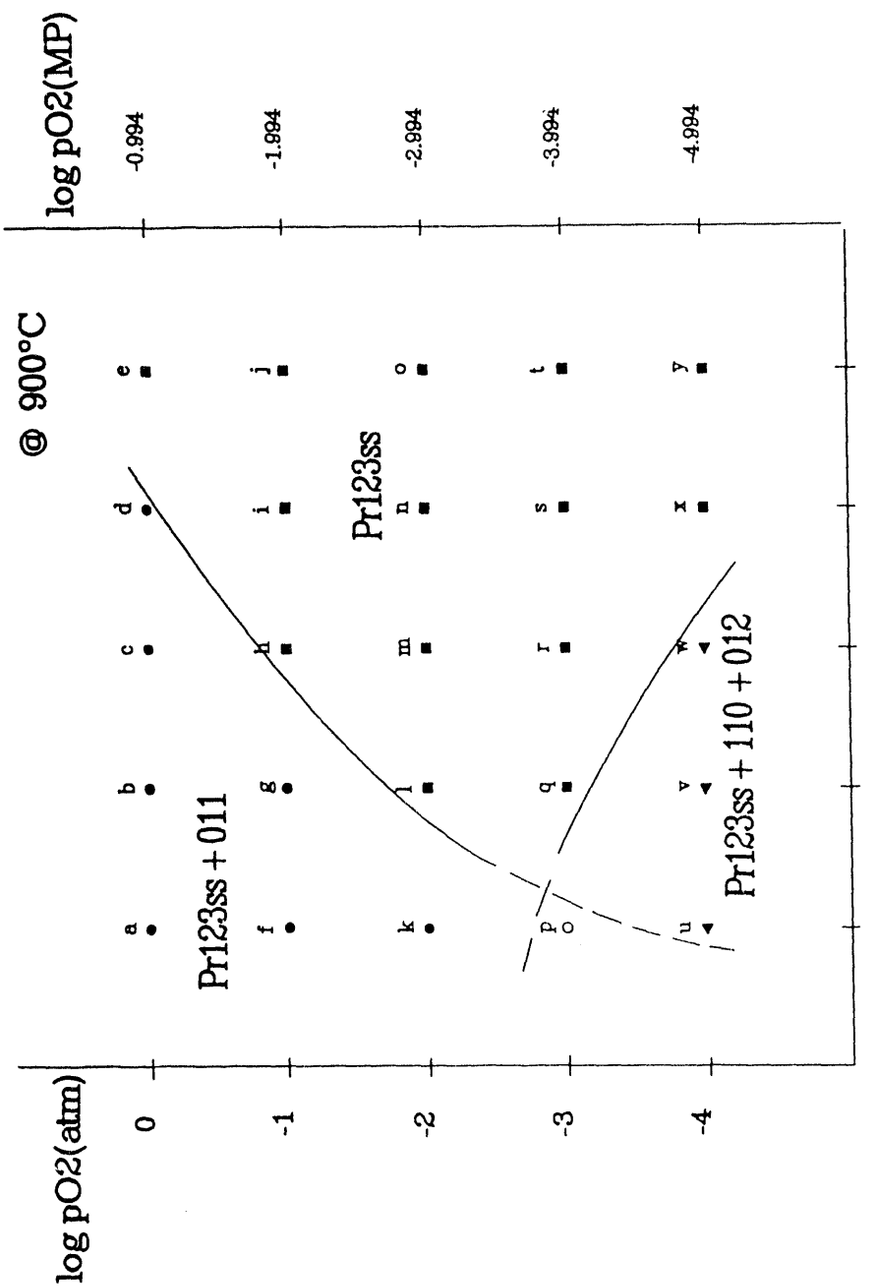

Figure 7 Phase diagram in the $Pr_{1+x}Ba_{2-x}Cu_3O_{7+\delta}$ (x= 0, 0.01, 0.02, 0.03, 0.04) as a function of PO_2 (log PO_2= 0, -1, -2, -3, -4)

Table 2 Nominal compositions of the samples, and phases observed (from Fig. 7)

SAMPLE NAME	COM-POSITION[%]	PROCESSING ATMOSPHERE	PHASES OBSERVED[*]	DTA ONSET (°C)	O_2 CONTENTS[#] b.o.	a.o.
a	1		123_{ss}, 011			
b	2		123_{ss}, 011			
c	3	100%O_2	123_{ss}, 011			
d	4		123_{ss}, 011			
e	5		123_{ss}			
f	1		123_{ss}, 011			
g	2		123_{ss}, 011			
h	3	10%O_2(in N_2)	123_{ss}			
i	4		123_{ss}			
j	5		123_{ss}			
k	1		123_{ss}, 011	924, 943	6.53	7.16
l	2		123_{ss}		6.53	7.33
m	3	1%O_2(in N_2)	123_{ss}		6.69	7.22
n	4		123_{ss}		6.48	7.33
o	5		123_{ss}		6.43	7.23
p	1		123_{ss}, 011, 110, 012	915, 936		
q	2		123_{ss}			
r	3	0.1%O_2(in N_2)	123_{ss}			
s	4		123_{ss}			
t	5		123_{ss}			
u	1		123_{ss}, 110, 012	925, 940		
v	2		123_{ss}, 110, 012			
w	3	0.01%O_2(in N_2)	123_{ss}, 110, 012			
x	4		123_{ss}			
y	5		123_{ss}			

[*] 123_{ss}=$Pr_{1+x}Ba_{2-x}Cu_3O_{7+\delta}$, 011=$BaCuO_2$, 110=$PrBaO_3$, 012=$BaCu_2O_2$
[%] 1=Pr123, 2=Pr1.01-1.99-3, 3=Pr1.02-1.98-3, 4=Pr1.03-1.07-3, 5=Pr1.04-1.96-3
[#] b.o. =before oxygenation, a.o. =after oxygenation

The Pr(O)-Cu(O) system Tetragonal Pr_2CuO_4 with the space group {I4/mmm} was formed in an ambient oxygen pressure [42]. It was found that Pr_2CuO_4 is stable at low oxygen partial pressures.

The pseudo-ternary system

In the RE(O)-Ba(O)-Cu(O) system, a solid solution occurs between the RE and Ba ions (RE=La, Pr, Nd, Sm, Eu, Gd). The ionic radii of the lanthanide ions decrease as we go from left to right in the periodic table. This phenomena is called "lanthanide contraction". Since the lattice mismatch increases as the RE ions become smaller, the degree of solid solubility decreases. Other RE ions have negligible solid solubility with Ba ions. Several authors claim that nominal Pr123 contains $BaCuO_2$ as an impurity phase [23,39,40]. This impurity must be produced by the formation of the solid solution $Pr_{1+x}Ba_{2-x}Cu_3O_{7+\delta}$ (where $x>0$), since there is a tendency for Ba sites to accommodate Pr ions. The $BaCuO_2$ phase did not disappear despite 10 days firing in an oxygen atmosphere. In order to determine the lower solubility limit in the $Pr_{1+x}Ba_{2-X}Cu_3O_{7-\delta}$ solid solution system, nominal Pr123 and $Pr_{1.05}Ba_{1.95}Cu_3O_{7+\delta}$ (Pr1.05-1.95-3) were prepared and their composition were confirmed by ICP-AES. Pr1.01-1.99-3, Pr1.02-1.98-3, Pr1.03-1.97-3, and Pr1.04-1.96-3 were obtained by mixing and heating the appropriate amount of these end point compounds (Pr123 and Pr1.05-1.95-3). As is seen in Fig. 8, the $BaCuO_2$ peak disappears at around $x=0.04$. The upper solubility limit is probably higher than $x=0.7$, although solid solutions with compositions higher than $x=0.7$ were not studied. These results were inconsistent with that of Hodorowicz et al. [25], who reported a solid solution range of $-0.1<x<0.55$.

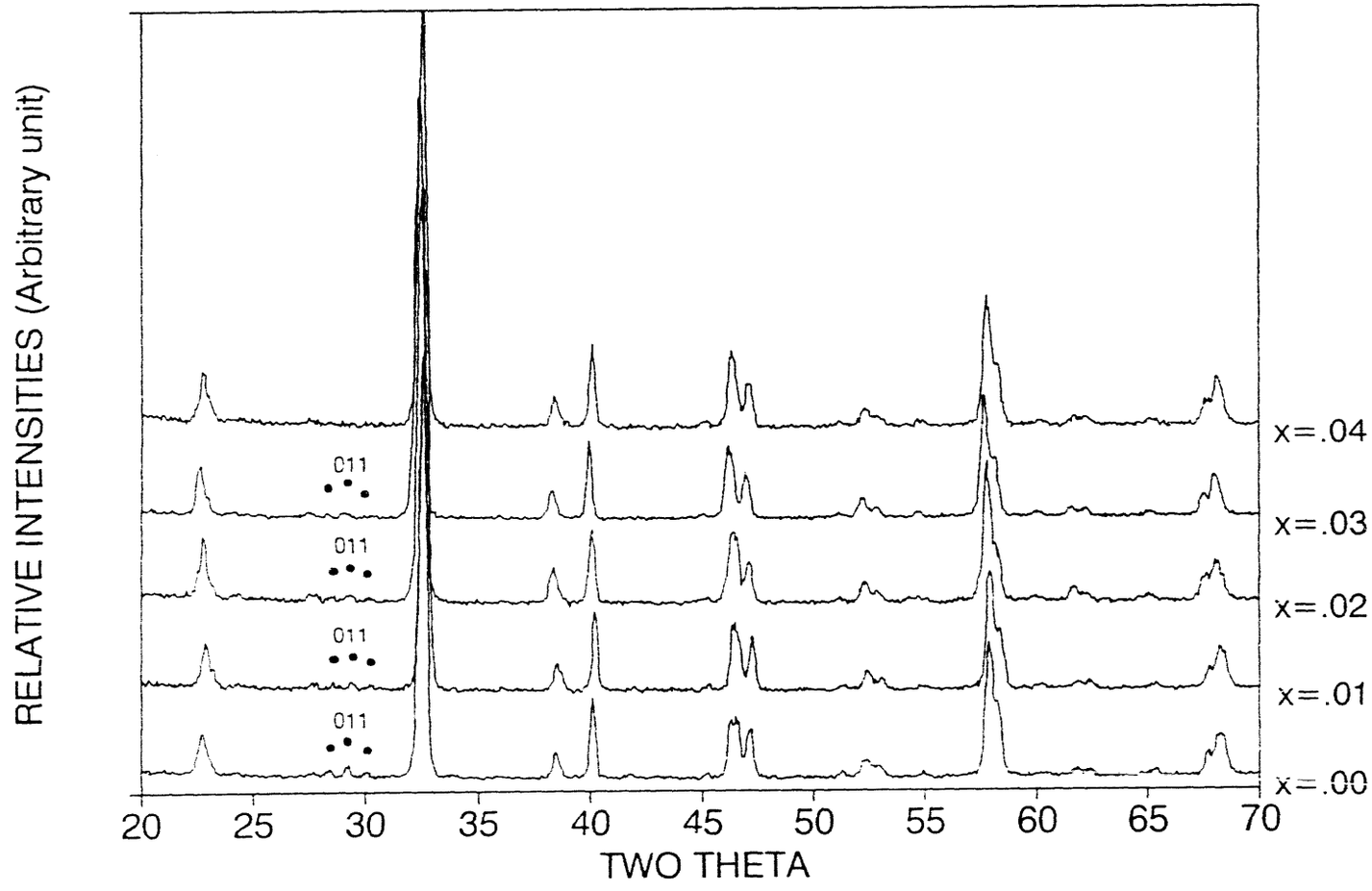

Figure 8 XRD data of $Pr_{1+x}Ba_{2-x}Cu_3O_{7+\delta}$ solid solutions where x = 0, 0.01, 0.02, 0.03, 0.04

Thermal events in the Pr-Ba-Cu-O system

Thermal events of the single phases

The melting events of single phase $Pr_{1.1}Ba_{1.9}Cu_3O_{7+\delta}$ (Pr1.1-1.9-3) were studied by DTA and XRD. Single phase Pr1.1-1.9-3 solid solution was used instead of the nominal Pr123 since nominal Pr123 contains $Pr_{1+x}Ba_{2-x}Cu_3O_{7+\delta}$ solid solution ($Pr123_{ss}$) plus $BaCuO_2$. A single endothermic event occurred at 975°C in air, as is shown in Fig. 9. In order to identify the nature of the reaction, the samples were heated to 990°C and quenched in air. The samples quenched from 990°C contained $Pr123_{ss}$, $PrBaO_3$, CuO, and Cu_2O. The $PrBaO_3$ must be a product of this reaction. The CuO and Cu_2O are possibly non-equilibrium products which were solidified from the remaining Pr-poor liquid by fractional crystallization. This situation is analogous to the Y123 system where non-equilibrium cooling produced several RE-poor compounds [43]. Based on these results, it is found that $Pr123_{ss}$ melts incongruently at 975°C in air producing $PrBaO_3$ and liquid;

$$Pr123_{ss} \text{ ---> } PrBaO_3 + L$$

Pr_2CuO_4 was found to decompose at 1258°C, and the melting temperature of $PrBaO_3$ was found to be higher than 1300°C.

Thermal events of the binary mixtures

$Pr123_{ss}$ - CuO Pr1.1-1.9-3 has been heated with excess amount of $BaCuO_2$ powder in the DTA furnace. An endothermic event was observed at 923°C[19], and 937°C[22], where the number inside the parenthesis indicates the composition of the sample described in Fig. 6. The material cooled from 940°C contained $Pr123_{ss}$, CuO, and Cu_2O. $Pr123_{ss}$ probably reacted with CuO producing a liquid;

$$Pr123_{ss} + CuO \text{ ---> } L$$

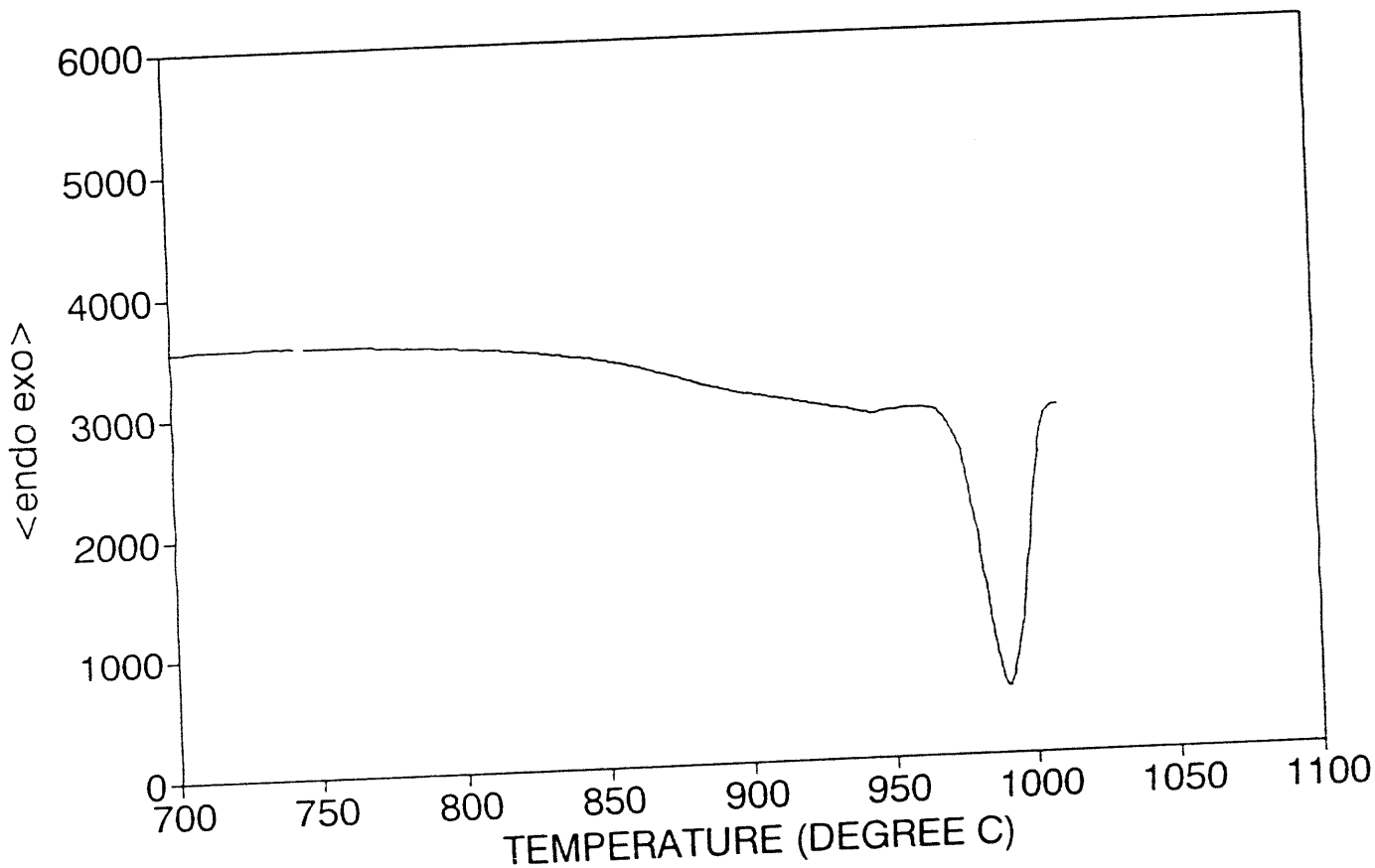

Figure 9 DTA endothermic event of $Pr_{1.1}Ba_{1.9}Cu_3O_{7+\delta}$

$Pr123_{ss}$ - $BaCuO_2$ In this system, an endothermic event occurs at 959°C[16],and 958°C[28]. Since the temperature of this thermal event is very close to that of the decomposition of $Pr123_{ss}$, the endothermic peaks due to both events were superimposed. In order to deconvolute these peaks, $Pr123_{ss}$ (hereafter called sample A) and a mixture of $Pr123_{ss}$ plus $BaCuO_2$ (hereafter called sample B) were heated to 970°C at the same time and air-quenched. Sample B was composed of $Pr123_{ss}$, CuO, $BaCuO_2$, $BaCu_2O_2$, and $PrBaO_3$. On the other hand, no reaction was found to exist in sample A up to that temperature. Therefore, it can be concluded that the reaction in sample B at 970°C is due to the reaction between $Pr123_{ss}$ and $BaCuO_2$, and not due to the decomposition of $Pr123_{ss}$, suggesting that;

$$Pr123_{ss} + BaCuO_2 \text{ ---> } PrBaO_3 + L$$

$Pr123_{ss}$ - $PrBaO_3$ Below 1300°C in air, no reaction, except the melting event of $Pr123_{ss}$, was observed in this system.

$PrBaO_3$ - $BaCuO_2$ No melting events besides that of $BaCuO_2$ was found to exist below 1300°C.

Thermal events of the ternary mixtures

Only the $Pr123_{ss}$-$BaCuO_2$-CuO system has been studied in this work. In order to promote the intimacy of these three phases, the mixture of powder was pre-heated to a temperature above the eutectic melting point of $BaCuO_2$ and CuO [33]. As a result, the transport of matter could be facilitated due to the formation of liquid. It was determined that $Pr123_{ss}$ reacts with $BaCuO_2$ and CuO producing liquid;

$$Pr123_{ss} + BaCuO_2 + CuO \text{ ---> } L$$

In addition to $Pr123_{ss}$, $BaCuO_2$, and CuO phases, a $BaCu_2O_2$ phase was observed in XRD results from the quenched sample.

Construction of the phase diagram at high temperature (above 880°C)

Thermal events in the Pr-Ba-Cu-O system are summarized in Table 3. Based on this research and analogy from other systems, the phase diagram of Pr-Ba-Cu-O at higher temperatures was constructed in Fig. 10. Isothermal sections at 920°C, 970°C, and 1000°C in air are also depicted. Above approximately 890°C, the region of eutectic liquid starts to expand as the temperature increases. Above 960°C, the tie-line between $Pr123_{ss}$ and $BaCuO_2$ disappears. $Pr123_{ss}$ finally decomposes into $PrBaO_3$ plus liquid at 974°C in air.

Phase diagram of the $Pr_{1+x}Ba_{2-x}Cu_3O_{7+\delta}$ as a function of PO_2.

Charge neutrality plays a very important role in ceramic systems. A defective structure can be produced in order to satisfy charge neutrality. In the RE-Ba-Cu-O system RE^{3+} ions tend to occupy Ba^{2+} sites, resulting in a disturbance in charge neutrality. This imbalance can be compensated for partially by reducing the valance of the copper metal and/or by absorbing oxygen ions on the O(5) sites [4]. If this oxygen uptake can be prevented by employing reducing oxygen pressures during the processing, the tendency for Ba sites to accommodate Pr ions can be reduced. The crystal structure of $Y_{1-x}Pr_xBa_2Cu_3O_7$ was studied by neutron diffraction as a function of x [28]. It was revealed that the normally vacant O(5) site in the basal plane becomes partially occupied by oxygen with increasing x in Y123. The O(5) site occupancy might imply the presence of the Pr ions on the Ba sites. The occupation of the trivalent rare-earth ions on the divalent Ba sites induce the oxygen take-up to occur to satisfy charge neutrality. Therefore, if the material is processed under low oxygen partial pressure (PO_2), the Pr ions can be prevented from occupying the Ba sites. As an example, the stoichiometric La123 phase can be stabilized

Table 3 Thermal events in the Pr-Ba-Cu-O system

Phase assemblage[$]	DTA onset (°C)	Reaction (in air)	Phases observed
Pr1.1-1.9-3[(7)]	975	123_{ss}- > 110+L	123,110,002,001[990°C]
Pr201[(25)]	1258		
Pr110[(26)]	no melting(below 1300°C)		
011[(27)]	1019	011- > L*	
80*m/o*123ss+20*m/o*001[(19)]	923		
14*m/o*123ss+86*m/o*001[(22)]	937	123_{ss}+001- > L	123_{ss},001,012[940°C]
70*m/o*123ss+30*m/o*011[(16)]	959		
32*m/o*123ss+68*m/o*011[(28)]	958	123_{ss}+011- > 110+L	123_{ss},001,011,012,110[970°C]
50*m/o*123ss+50*m/o*110[(29)]	974^	no reaction(below 1300°C)	
50*m/o*011+50*m/o*001[(30)]	902	011+001- > L*	
40*m/o*110+60*m/o*011[(13)]	1011#	no reaction(below 1300°C)	
10*m/o*123ss+67*m/o*001+23*m/o*011[(21)]	905&	123_{ss}+011+001- > L	123_{ss},001,012,011[910°C]
62*m/o*123*ss*+10*m/o*001+28*m/o*011[(18)]	891&		

$ **Pr1.1-1.9-3**=$Pr_{1.1}Ba_{1.9}Cu_3O_{7+\delta}$, **Pr201**=$Pr_2CuO_4$, **Pr110**=$PrBaO_3$
011=$BaCuO_2$, **123**$_{ss}$=Pr1.1-1.9-3, **001**=CuO
% **002**=Cu_2O, **012**=$BaCu_2O_2$
* ref [33]
& preheated at above e_2 temp
( ) sample composition (described in Fig. 6.)
[ ] temp. the samples were quenched from
^ due to the melting of 123ss
# due to the melting of 011

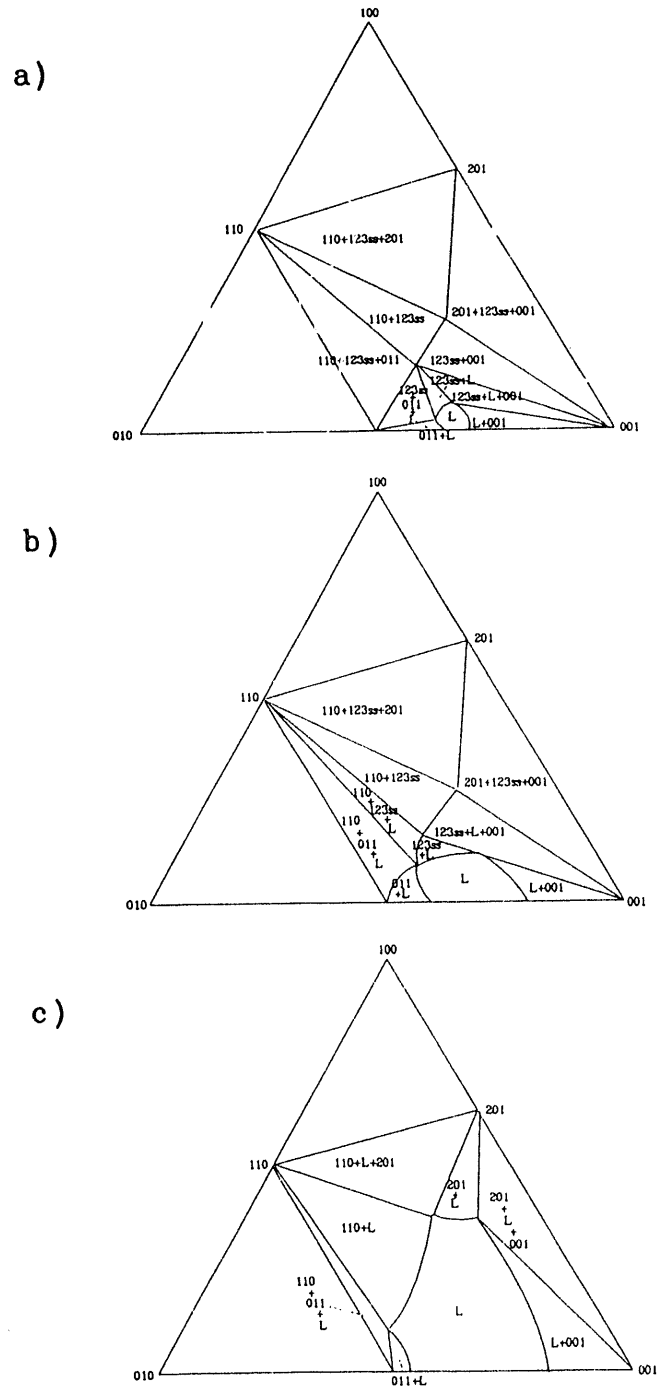

Figure 10 Construction of the phase diagram at high temperature (a) 920°C, (b) 970°C, (c) 1000°C

only when it is sintered at low oxygen pressures [44]. Similarly, as the PO_2 is lowered, the amount of $BaCuO_2$ in the $Pr123_{ss}$ system is significantly diminished; i.e. low PO_2 processing favors cation-site ordering.

Fig. 6 shows the phase diagram at 900°C as a function of the oxygen partial pressure. The nominal compositions of the samples and the phases observed are summarized in Table 2. By lowering the oxygen partial pressure to 0.01-0.001 atm the single phase region is expanded. However, as the PO_2 is lowered below 0.01-0.001 atm, $BaCu_2O_2$ and $PrBaO_3$ were found as second phases. Based on these results, the following reaction equations were suggested;

Above 0.01-0.001 atm PO_2, the amount of $BaCuO_2$ decreases with decreasing PO_2.

$$\mathbf{PrBa_2Cu_3O_c + [\epsilon/2]O_2 \Rightarrow [1/(1+x)]Pr_{1+x}Ba_{2-x}Cu_3O_{c+x/2} + [3x/(1+x)]BaCuO_2}$$

$$\epsilon = \frac{\mathbf{x(6.5-c)}}{\mathbf{(1+x)}} \qquad \text{(above 0.01-0.001 atm } PO_2\text{)}$$

where c is the critical oxygen content of the sample at equilibrium with 0.01-0.001 atm PO_2, ϵ is the excess oxygen content which is added to or subtracted from the system. It was assumed that c is a constant. The formula of $\epsilon = f(x)$ was calculated from the consideration of the stoichiometry of oxygen atoms. It can be viewed that equilibrium oxygen content of the sample is a function of PO_2. Increase in PO_2 in the atmosphere result in addition of oxygens into the system, increasing the value of ϵ; i.e., as PO_2 increases, ϵ increases. From the relationship between ϵ and x, it can be seen that x increases as ϵ increases.

Similarly, below 0.01-0.001 atm PO_2, the amounts of $BaCu_2O_2$ and $PrBaO_3$ increase with decreasing PO_2.

$$\mathbf{PrBa_2Cu_3O_c + [\epsilon/2]O_2 => [1/(1+4x)]Pr_{1+x}Ba_{2-x}Cu_3O_{c+x/2} + [6x/(1+4x)]BaCu_2O_2 + [3x/(1+4x)]PrBaO_3}$$

$$\epsilon = \frac{x}{(1+4x)}(21.5-4c) \qquad \text{(below 0.01-0.001 atm } PO_2\text{)}$$

That is to say, as ϵ decreases, x increases. Noted that the value of c ranges between 5.33 and 6.5. This is argument is plausible since the equilibrium oxygen content at 900°C in around 0.01-0.001 atm PO_2 in the Pr123 system is approximately lower than 6.2 and higher than 6.0, which can be deduced from the Y123 system [57]. However, compared to Pr123 system, Y123 is unstable at 900°C if PO_2 is lower than 0.01 atm.

Based on this result, an isothermal section of the phase diagram at 0.0001 atm PO_2 was constructed in Fig. 11. At this atmosphere, $BaCu_2O_2$ and Cu_2O are stable. $PrBaO_3$ and Pr_2CuO_4 were found to be stable even in a nitrogen atmosphere. The $Pr_{1+x}Ba_{2-x}Cu_3O_{7-\delta}$ solid solution region did not disappear at this atmosphere.

Since the major impurity phase which appears in this system is $BaCuO_2$, it is important to understand the reaction between $Pr123_{ss}$ and $BaCuO_2$ as a function of oxygen partial pressure. The temperature of this reaction is lowered by reducing the PO_2, as is seen in Fig. 12. The peak due to this reaction and that of the melting of Pr123 start to split. In order to insure that the phases present, other than 123_{ss}, were not produced by any invariant reaction, thermal analysis was performed on the samples processed at PO_2's lower than 0.1 atm. No evidence was found for melting events before 900°C at these

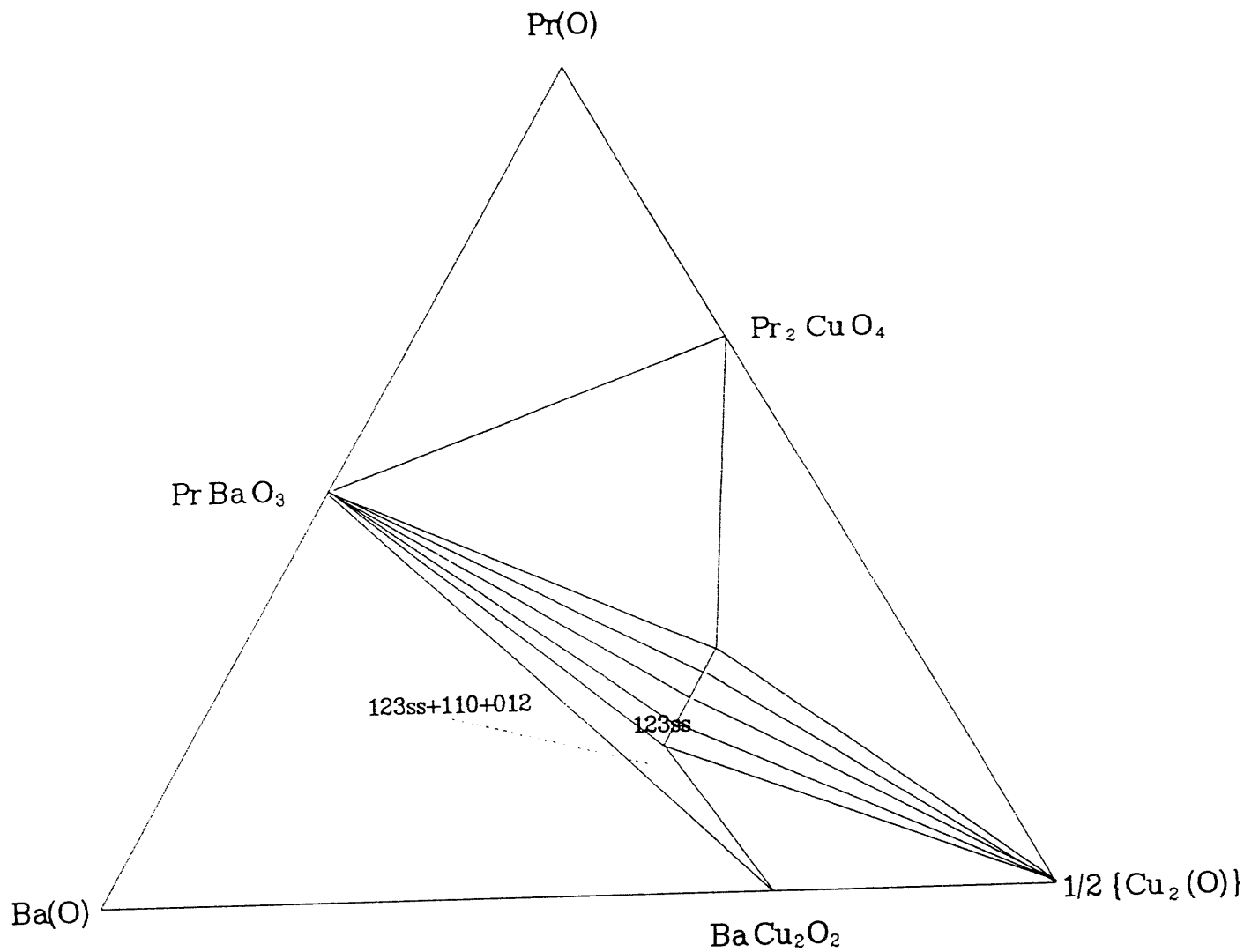

Figure 11 Isothermal section of the phase diagram of Pr-Ba-Cu-O at 0.0001 atm PO_2 at 900°C

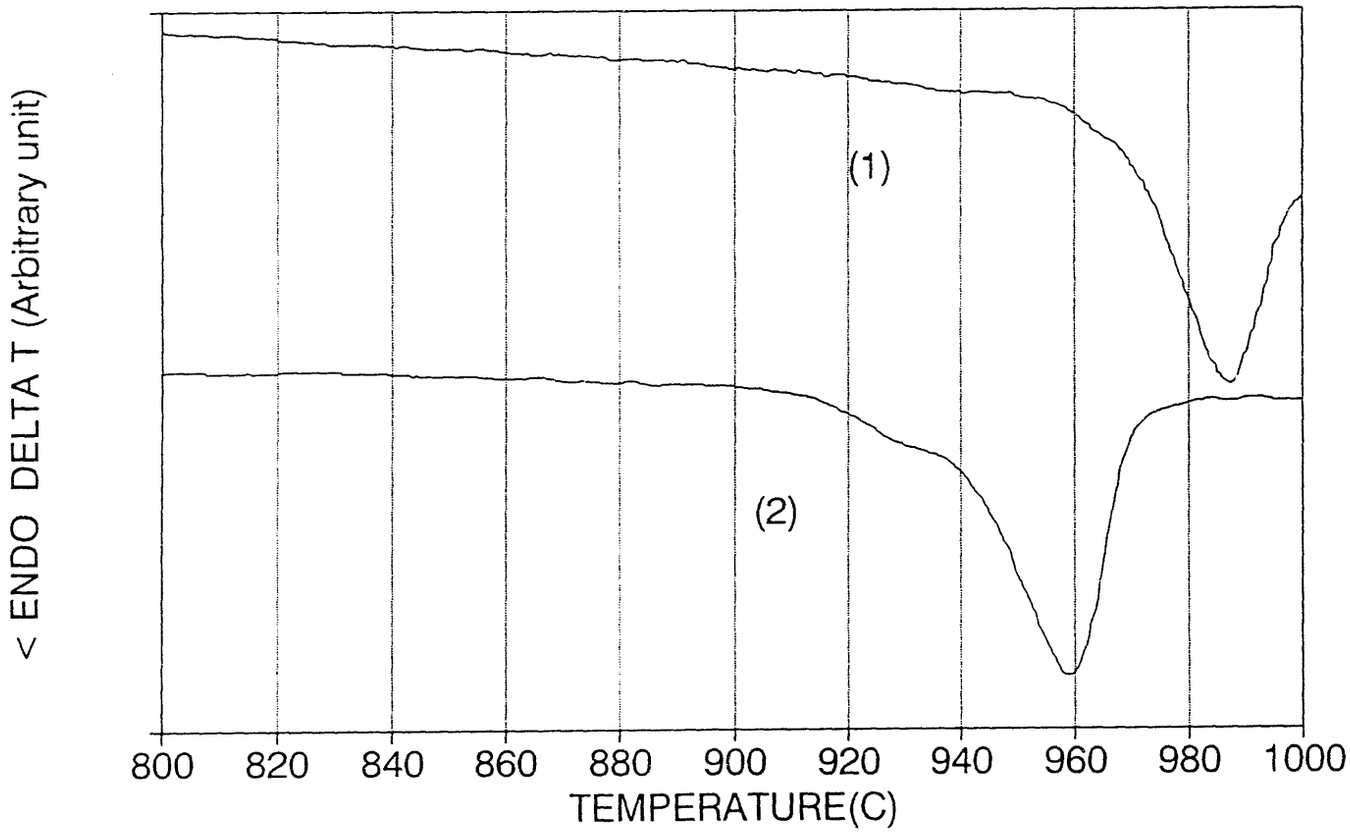

Figure 12 DTA endotherms of the Pr123 plus $BaCuO_2$ mixture at different PO_2 (1):1 atm, (2):0.01 atm

atmospheres. It was found that sample 'p' (from the Fig. 7) contained four condensed phases. The phase rule at a fixed temperature is given by,

$$f = c - p + 1$$

where f is the degrees of freedom, c is the number of the components, and p is the number of phases. In this system c can be taken as four. Since the point 'p' contained four condensed phases and a gas phase, f is zero. Therefore, the region around point 'p' is a non-equilibrium region. The oxygen stoichiometry of the samples before and after oxygenation are tabulated in Table 2. As is seen in the other RE-Ba-Cu-O systems, oxygenation does increase oxygen content. The lattice constants of the samples were determined and tabulated in Table 4.

Magnetic properties of the Pr-Ba-Cu-O system

Fig. 13(a) and 13(b) show the inverse susceptibility versus temperature curve of Pr1.01-1.99-3 processed in 0.001 and 0.21 atm oxygen, respectively. From the Curie-Weiss law;

$$\frac{1}{X} = \frac{T - \Theta}{C}$$

where, Θ and C are the Curie temperature and Curie constant, respectively. Since Θ has a negative value with this data, the nature of the magnetic ordering is antiferromagnetic. Compared to other reports [11], and the material heat-treated at 0.21 atm PO_2 , the material processed at 0.001 atm has a higher T_N (18.5K). One possible explanation for this fact is that low PO_2 processing may induce better cation-site ordering and produce magnetic ordering at a higher temperature. In the Pr-rich $Pr_{1+x}Ba_{2-x}Cu_3O_{7+\delta}$ solid-solution, the magnetic properties of Pr1.7-1.3-3 were investigated. Fig. 13(c) shows that

Table 4 Lattice constants of the samples (from Fig. 7)

SAMPLE NAME	LATTICE CONSTANTS (A) a	b	c	UNIT CELL VOLUME	ORTHORHOMBICITY $\Phi = \sqrt{(1-(a/b)^2)}$
k(deoxygenated)	3.907(3)		11.869(11)	181.2(.2)	
k(oxygenated)	3.854(4)	3.919(10)	11.753(17)	177.5(.4)	0.1814
l(deoxygenated)	3.908(2)		11.870(8)	181.3(.1)	
l(oxygenated)	3.842(4)	3.930(10)	11.760(15)	177.5(.4)	0.2106
o(deoxygenated)	3.905(1)		11.861(5)	180.9(.1)	
o(oxygenated)	3.857(4)	3.922(4)	11.721(14)	177.3(.3)	0.1809

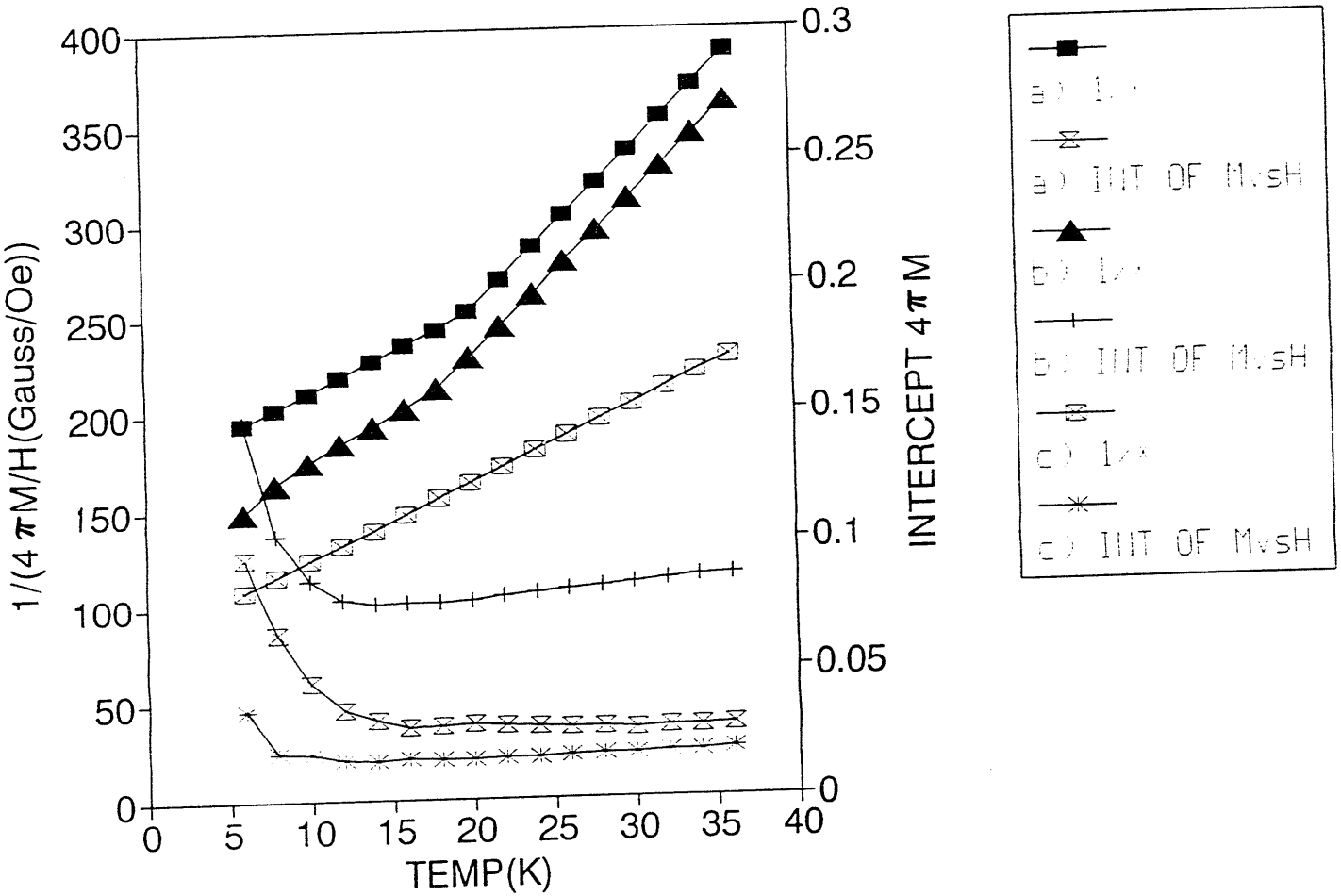

Figure 13 Inverse susceptibility vs temperature of (a) Pr1.01-1.99-3 [0.001 atm], (b) Pr1.01-1.99-3 [0.21 atm], and (c) Pr1.7-1.3-3 [0.21 atm]

this material does not show any deviation from the Curie-Weiss law down to 6K, which is a good agreement with results from other literature [45]. By comparing this graph with that of Fig. 13(a) or 13(b), it can be concluded that the occupation of the Pr ions on the Ba site destroys magnetic ordering of the Pr ions. The Neel temperature, T_N, Curie constant, C, and paramagnetic Curie temperature, Θ of theses samples are comparared in Table 5.

The graph in Fig. 14 shows a deviation from Curie-Weiss behavior below 15K in $PrBaO_3$. This magnetic ordering temperature is in agreement with the results of the neutron scattering study [41]. Since $PrBaO_3$ was found as a major impurity phase in the low PO_2 processed sample, it would be interesting to study the magnetic properties of this material. Due to the difference in T_N between Pr123 and $PrBaO_3$, the presence of $PrBaO_3$ in the sample may be identified.

Table 5 Comparison of Neel temperature, T_N, Curie constant, C, and paramagnetic Curie temperature, Θ of the samples

Sample Name	Processing PO_2	T_N	C	$-\Theta$
Pr1.01-1.99-3	0.001 atm	18.5K	0.12	10.01K
Pr1.01-1.99-3	0.21 atm	17.0K	0.12	7.70K
Pr1.7-1.3-3	0.21 atm	< 6.0K	0.25	21.00K

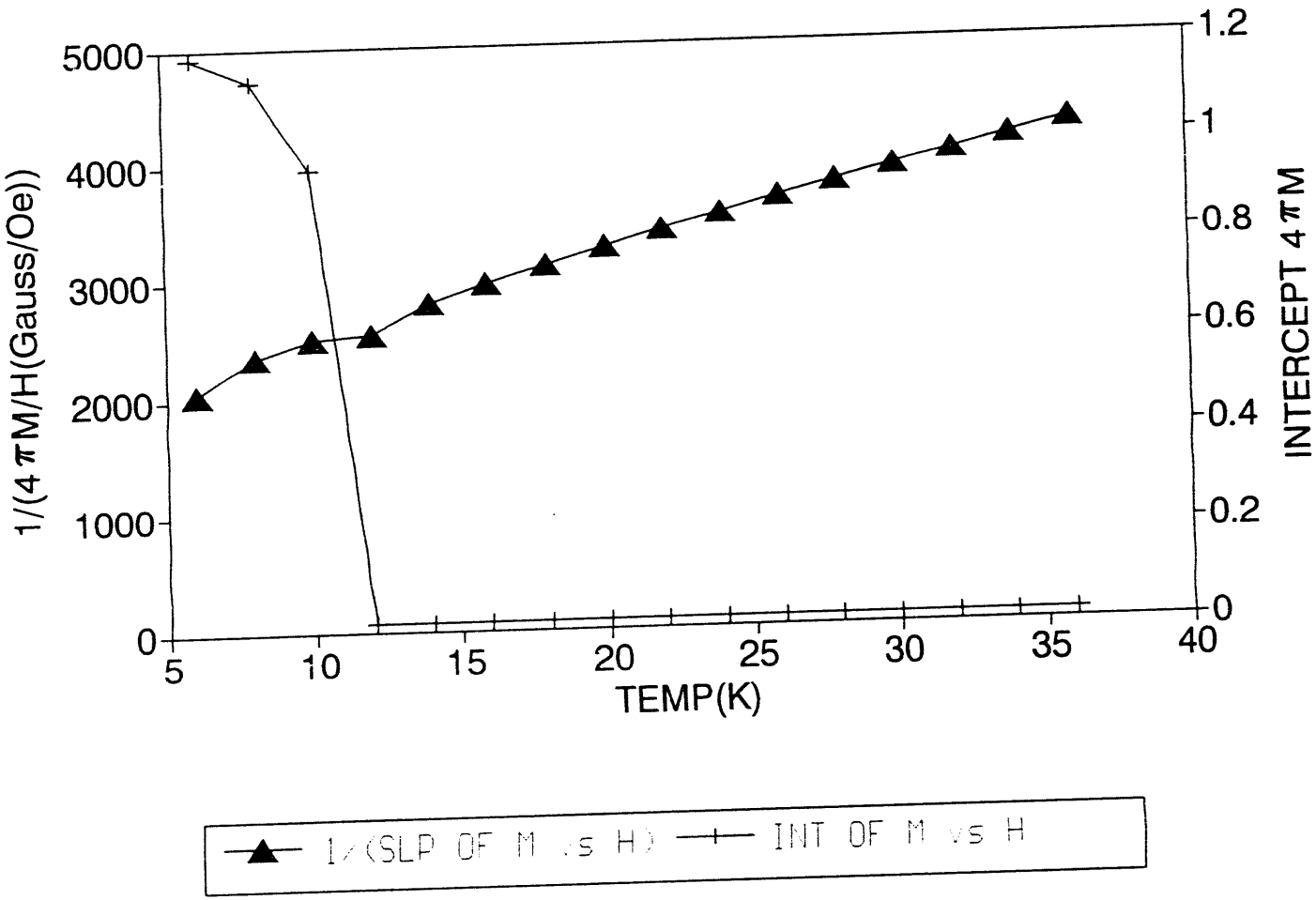

Figure 14 Inverse susceptibility vs temperature curve of $PrBaO_3$

CONCLUSIONS

The important findings in this study can be summarized as follows;

1) The stoichiometric Pr123 does not exist in air. Instead, nominal Pr123 is a mixture of $Pr123_{ss}$ and $BaCuO_2$.

2) By lowering the oxygen partial pressure during heat-treatment, the Pr ions can be prevented from occupying Ba sites. However, the occupation of Pr on the Ba sites cannot be completely suppressed even at low PO_2's. Further reducing the PO_2 causes other second phases to form. Above 0.01-0.001 atm PO_2, the amount of $BaCuO_2$ decreases with decreasing PO_2. Below 0.01-0.001 atm PO_2, the amounts of $BaCu_2O_2$ and $PrBaO_3$ increases with decreasing PO_2.

3) $Pr123_{ss}$ processed at a low PO_2 has a higher antiferromagnetic ordering temperature ($T_N = 18.5K$). This is probably due to the fact that low PO_2 processing favors cation-site ordering.

In conclusion, the amounts of Pr ions which occupy the Ba sites can be minimized by processing the material at low PO_2 (0.01-0.001 atm)

PART 2. STRUCTURE AND SUPERCONDUCTIVITY OF $Nd_{1-x}Pr_xBa_2Cu_3O_{7-\delta}$

INTRODUCTION

One method of investigating superconductivity in the Pr-Ba-Cu-O system is to compare this system with other superconducting RE-Ba-Cu-O systems by forming a solid-solution. Among RE-Pr-Ba-Cu-O solid-solution systems, the Nd-Pr-Ba-Cu-O system is especially interesting because the size of the Nd and Pr ions are similar and they are neighboring elements in the periodic table. Therefore, any effects caused by the size difference of these ions can be eliminated. The $Nd_{1-x}Pr_xBa_2Cu_3O_{7-\delta}$ system has been investigated by several groups [29-31], however, no magnetic susceptibility study in the Nd-rich region has been done. In general, magnetic susceptibility measurements are more sensitive than resistivity measurements. According to their results, the superconducting transition temperature, T_C, decreases monotonically with increasing x, and superconductivity disappears at around $x=0.3$. There is a slight disagreement on the actual shape of the T_c depression curve, although the general trend is the same.

In this research, the structure and superconducting properties of Nd-rich $Nd_{1-x}Pr_xBa_2Cu_3O_{7-\delta}$ ($x=0.1$, 0.2, 0.3, 0.4, 0.5) has been studied. Special processing methods were employed in this experiment in order to maximize the homogeneity of the samples. First, $(Nd_{1-x}Pr_x)_2CuO_4$ compounds were used as precursor materials in order to achieve intimate contact between Nd- and Pr-contained particulates. Second, $NdPr123_{ss}$ was synthesized at a low oxygen partial pressure since low PO_2 processing favors cation site ordering between RE (RE=Nd, Pr) and Ba. A detailed explanation of this method is contained in the 'experimental procedure' section.

RESULTS AND DISCUSSION

On structure

Fig. 15 shows the lower-angle region of the XRD pattern with 1%O_2-processed samples of x=0.1, 0.2, 0.3, 0.4, 0.5 in $Nd_{1-x}Pr_xBa_2Cu_3O_{7-\delta}$. $PrBaO_3$ was found as a second phase in the sample with x=0.5, which can be expected from the phase equilibria study. In the Nd-free $PrBa_2Cu_3O_{7+\delta}$ system, the extra Pr ions tend to occupy the Ba sites at low PO_2 (below 0.01-0.001 atm), producing $BaCu_2O_2$ and $PrBaO_3$ as second phases. At ambient atmosphere $BaCu_2O_2$ is unstable and decomposes into $BaCuO_2$ and CuO. Although the phase equilibria of the Pr-Ba-Cu-O system is different from that of the Nd-Pr-Ba-Cu-O system, an analogy can be made between the two systems if the Pr-rich region of the solid solution is considered; i.e. as the amount of Pr ions increases in the Nd-Pr-Ba-Cu-O solid-solution, the phase equilibria of this system resembles that of Pr-Ba-Cu-O. Therefore, it is believed that the degree of cation-site disorder of $PrBa_2Cu_3O_{7-\delta}$ is higher than that of $NdBa_2Cu_3O_{7-\delta}$.

In general, single crystals are preferred for the study of crystal structure since single crystals are an ideal form of the material. However, single crystals contain micro-twinned regions [46], and are not always available. Therefore, most of the time polycrystalline samples have to be used for crystal structure analysis. One of the drawbacks of using polycrystalline powder diffraction patterns is that higher angle peaks are usually highly superimposed. This phenomena is much more severe in the case of a sample which has a low crystal symmetry. Through the development of the structural refinement method by Rietveld [47,48], and computer programs for its utilization, powder

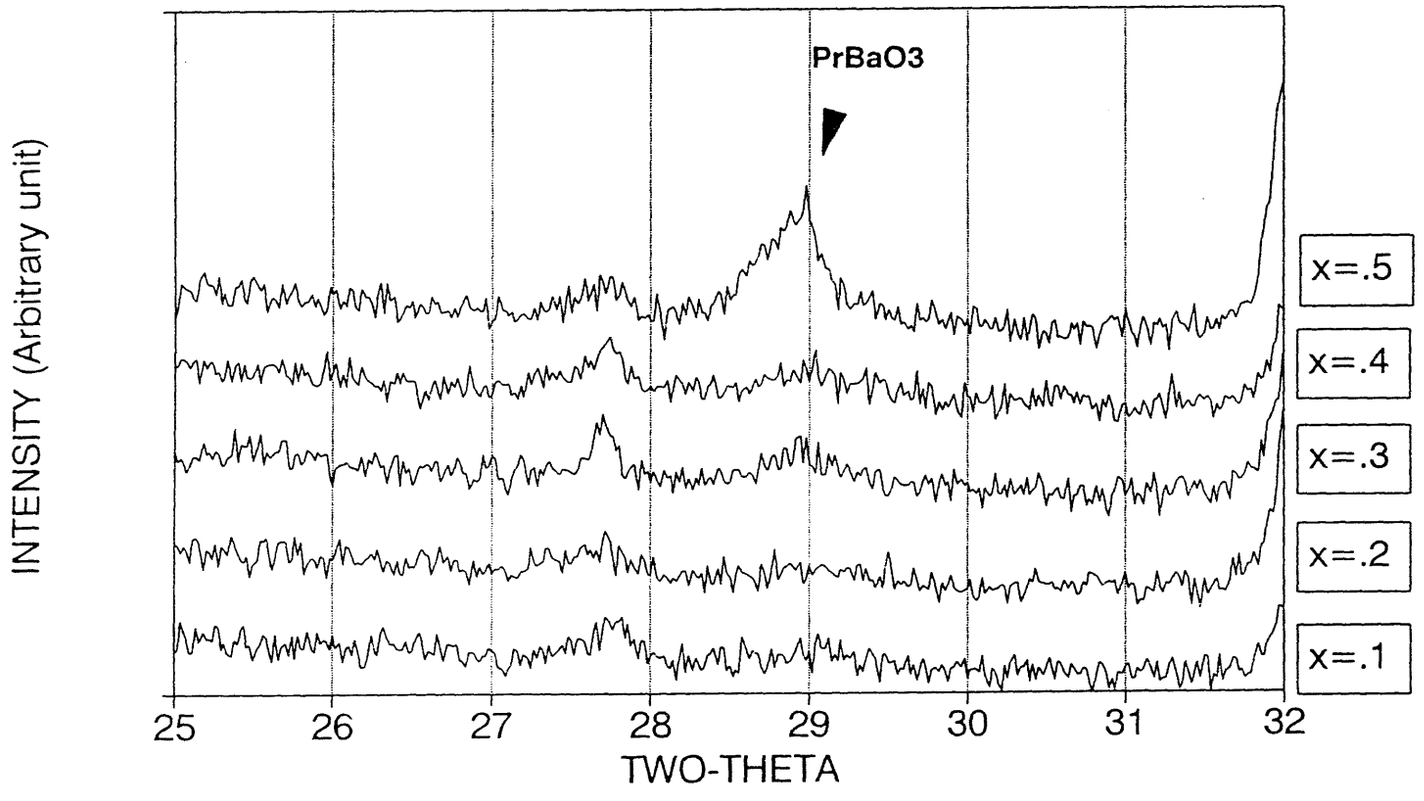

Figure 15 Lower-angle region of XRD pattern of 1%O_2-processed NdPr123$_{ss}$ (x in $Nd_{1-x}Pr_xBa_2Cu_3O_{7-\delta}$)

diffraction method can now compete with the single crystal methods. The major advantage of the Rietveld refinement method is that the peak overlap problem can be alleviated by using the entire diffraction pattern. This is in contrast to profile-fitting methods where observed peaks should be deconvoluted. In Rietveld refinement, all the data points are observations and several parameters are refined simultaneously. Least square procedure is performed until best fit between observed pattern and calculated model is obtained.

Rietveld analysis was performed on the orthorhombic RE-Ba-Cu-O structure which has a space group Pmmm. The designation of the atom position which was used as a starting model is described in Table 6. It was assumed that the O(5) sites were not occupied by the oxygen ions. Fig. 16 shows changes in lattice parameters as a function of x. All of the lattice constants in this plot were refined following the same refinement procedure. The values of a and b remain almost unchanged throughout the solid-solution range. The value of c changes anomalously in the x=0.3-0.4 region, where superconductivity disappears. It seems that the destruction of superconductivity is related to the change in size of the unit cell in the c direction. The change in c value possibly implies a change in the distribution of the cations along the [1/2 1/2 1] direction in the unit cell. From a consideration of the shape of the graph, it is plausible to consider that two structural changes are competing with each other in this system. One process decreases the c value and the other process slightly increases the c value as x increases in $Nd_{1-x}Pr_xBa_2Cu_3O_{7-\delta}$. At the Nd-rich region, the former process seems to be dominant, which might be related to the depression of T_c. However, at this point it is not certain what exact mechanism is governing in this process, it is plausible to think that there might be a relationship between this structural change and T_c depression.

Table 6 The designation of atom position in the unit cell which was used as a starting model

ATOM	X	Y	Z	FRAC
1) Nd	0.5	0.5	0.5	1-x
2) Ba	0.5	0.5	0.18	1
3) Cu(1)	0.0	0.0	0.0	1
4) Cu(2)	0.0	0.0	0.35	1
5) O(1)	0.0	0.5	0.0	1
6) O(2)	0.5	0.0	0.37	1
7) O(3)	0.0	0.5	0.38	1
8) O(4)	0.0	0.0	0.17	1
9) Pr	0.5	0.5	0.5	x

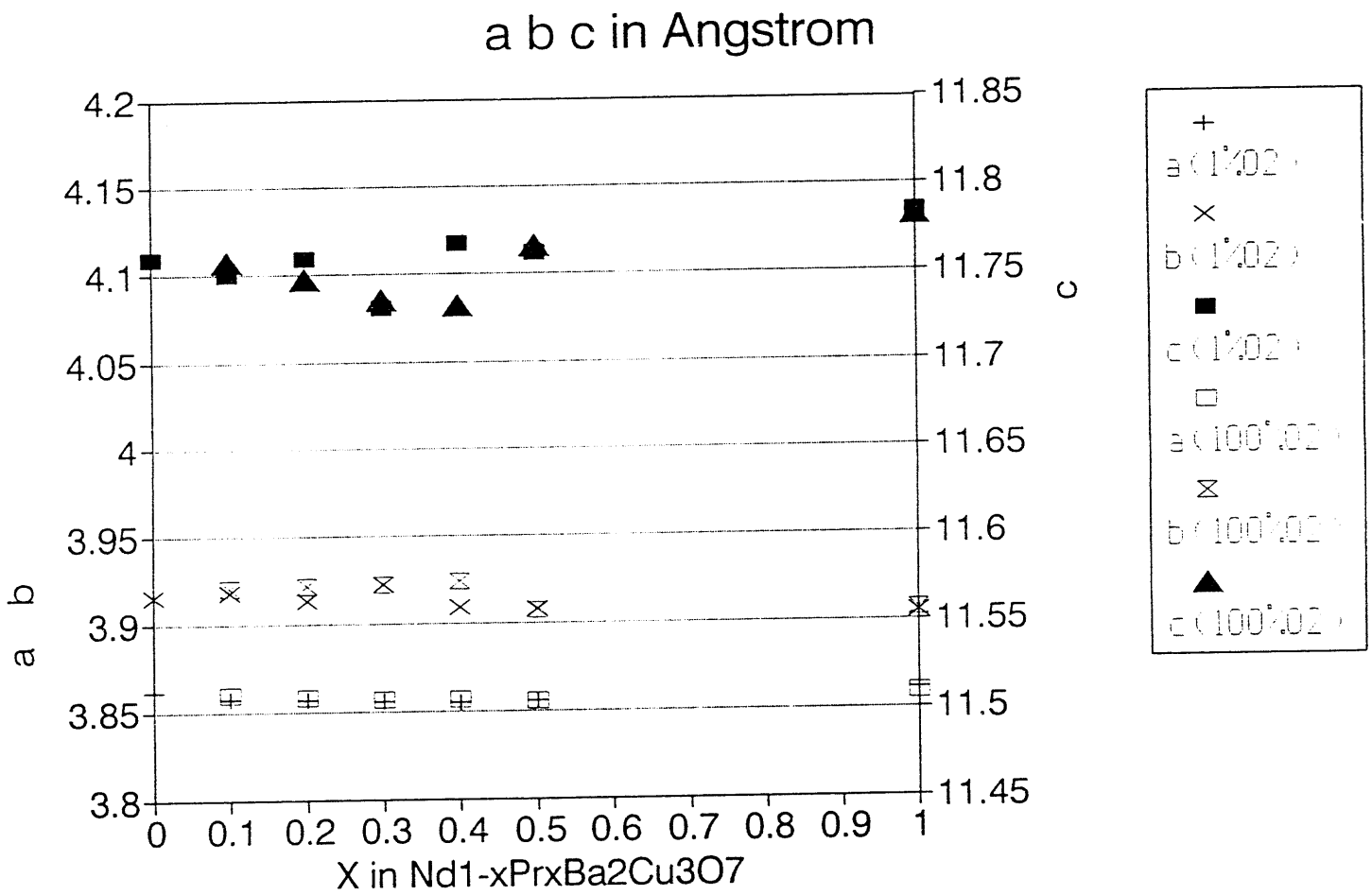

Figure 16 Change in lattice parameters of $Nd_{1-x}Pr_xBa_2Cu_3O_{7-\delta}$ (The sample with x=0 was prepared by A. Karion.)

On properties

Fig. 17, 18, and 19 show superconducting transition curves for $Nd_{0.9}Pr_{0.1}Ba_2Cu_3O_{7-\delta}$, $Nd_{0.8}Pr_{0.2}Ba_2Cu_3O_{7-\delta}$, and $Nd_{0.7}Pr_{0.3}Ba_2Cu_3O_{7-\delta}$, respectively. In order to improve the sensitivity of the measurements, the diamagnetic moment, not resistivity, of the sample was measured to determine the superconducting transition temperature, T_c. The so called 'magnetic T_c' measurement is advantageous over the standard four-probe method because very small resistances are difficult to measure and zero-resistance is practically impossible to measure. However, minute diamagnetic signals can be detected by using a SQUID magnetometer. As can be seen from these figures, T_c is increased by approximately 10K when the oxygen partial pressure during the processing was decreased to 0.01 atm. This is possibly due to the minimization of the occupancy of the extra RE ions on the Ba sites and paired occupation of the extra Pr ions on the Ba sites, which will be discussed later.

The sharp transition in T_c implies that these samples are fairly homogeneous. It is believed that this homogeneity in solid solution was achieved by high temperature heat-treatment of the precursor NdPr201s. Both the Nd and Pr ions must be homogeneously distributed throughout the sample without forming clusters of certain types of rare-earth ions. If an inhomogeneous solid solution is formed, a broad transition in Tc occurs since the Tc varies from region to region.

As is seen in Fig. 17, 18, and 19, the zero-field-cooled moment has a higher value than predicted. This discrepancy can be corrected, if the correct value of the demagnetization field is used. However, for polycrystalline ceramic sample, the demagnetization factor can hardly be defined. A superconducting fraction of the samples, the Meissner fraction (MF), can be expressed by

$$MF = -4\pi M / (H-H_d)$$

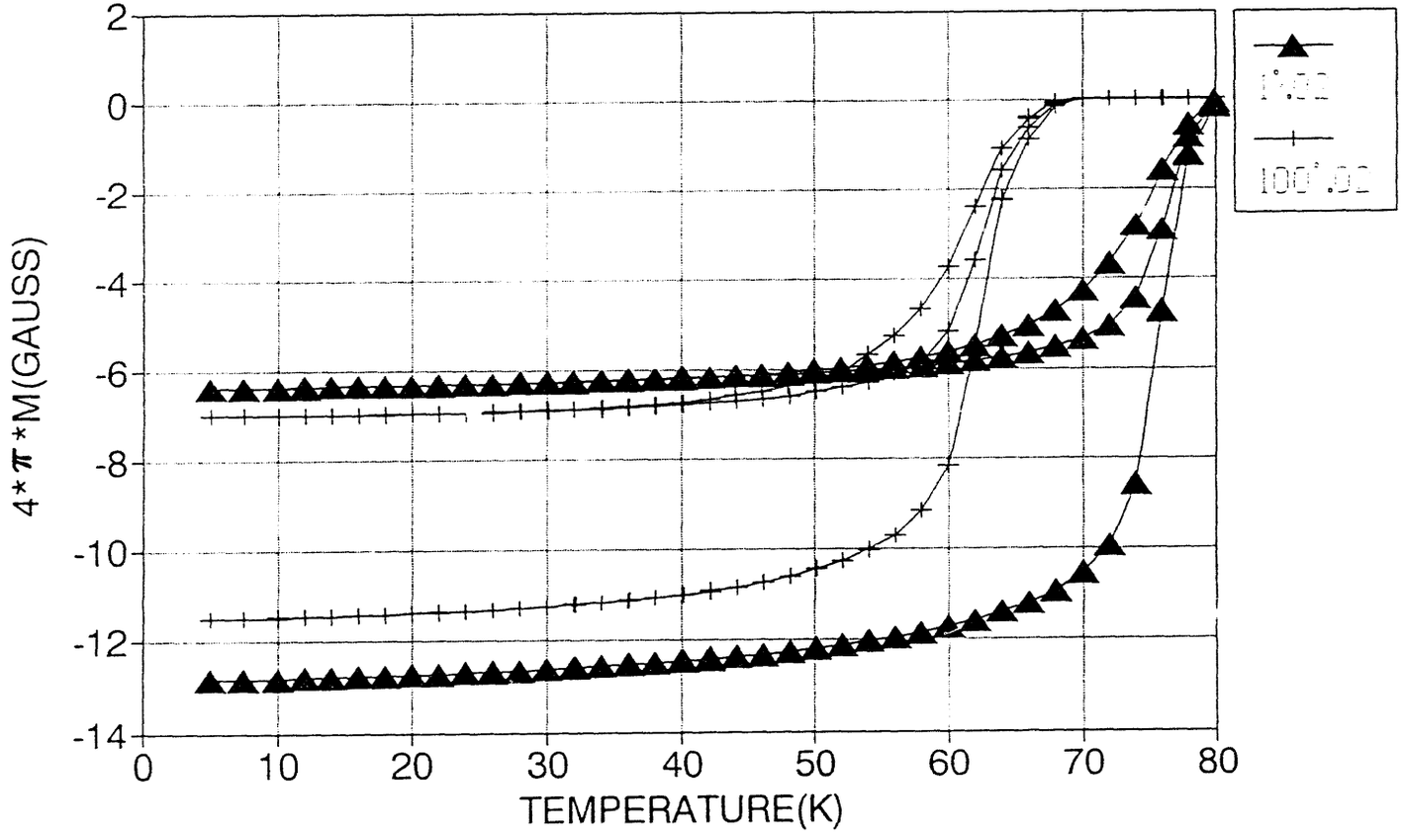

Figure 17 Superconducting transition curve of $Nd_{0.9}Pr_{0.1}Ba_2Cu_3O_{7-\delta}$

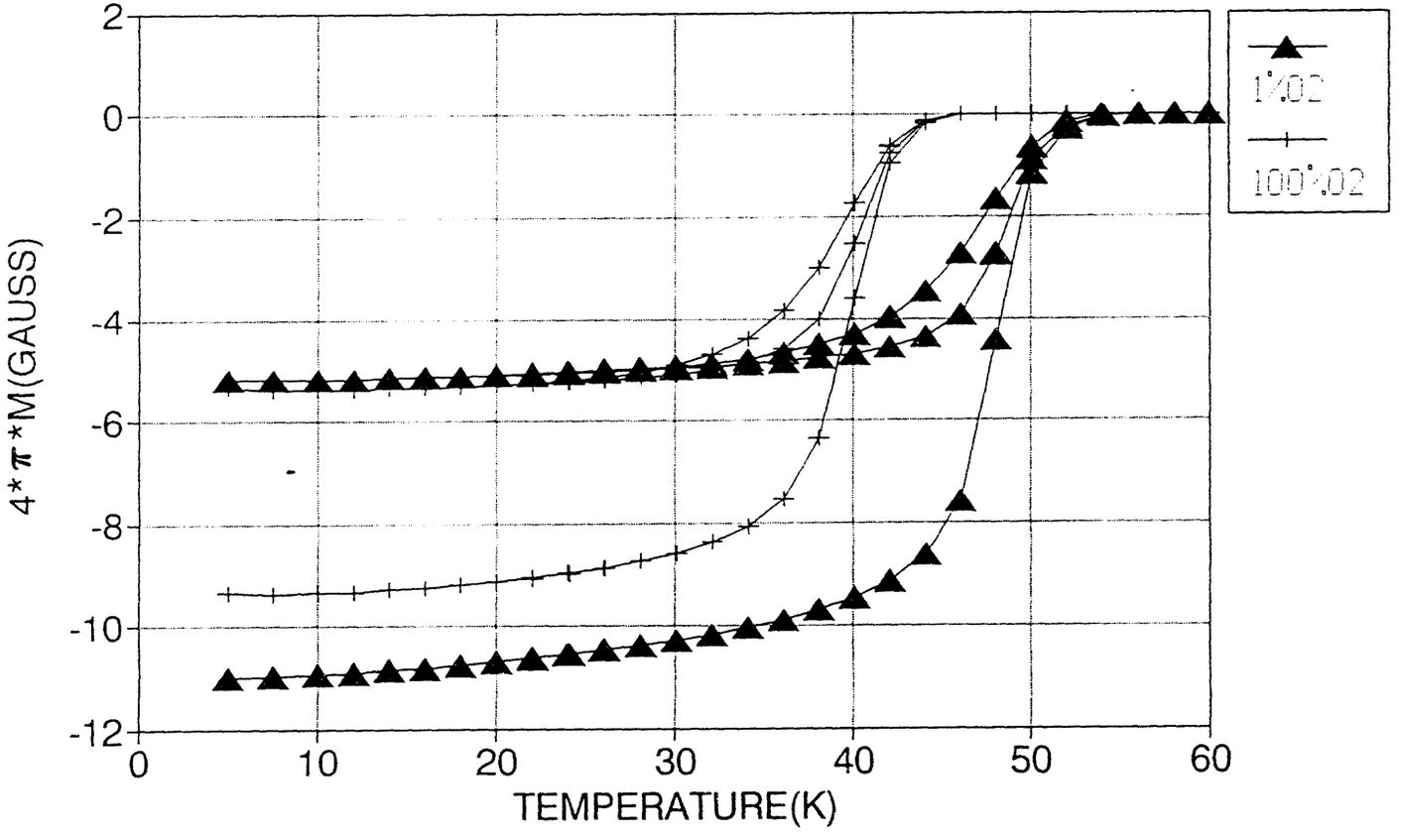

Figure 18 Superconducting transition curve of $Nd_{0.8}Pr_{0.2}Ba_2Cu_3O_{7-\delta}$

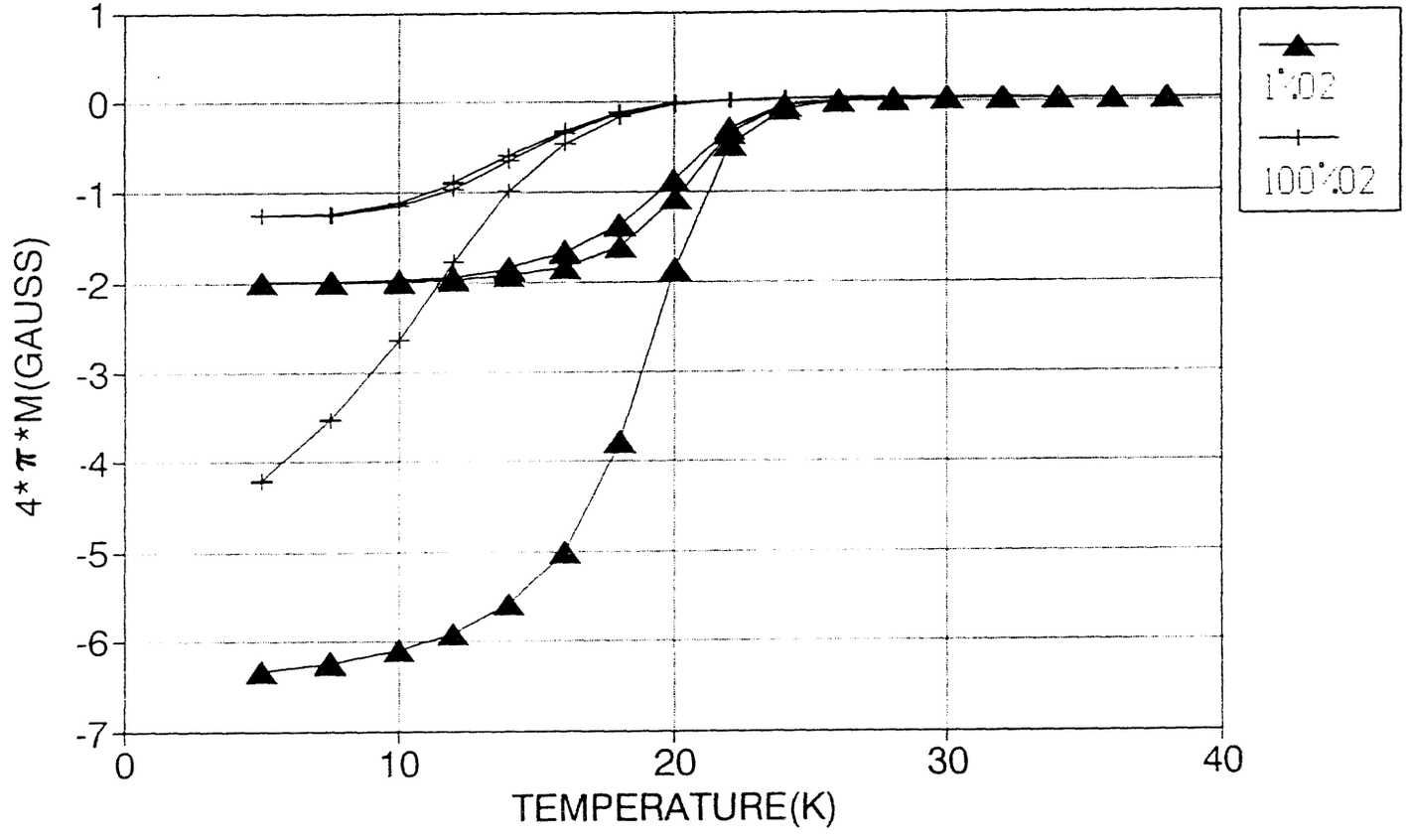

Figure 19 Superconducting transition curve of $Nd_{0.7}Pr_{0.3}Ba_2Cu_3O_{7-\delta}$

where H is the applied magnetic field, and H_d is the demagnetization field. Ideally, if the entire sample is superconducting, both the zero-field-cooled and field-cooled susceptibilities should be identical, and their values should approach $-1/4\pi$. However, the field-cooled susceptibility is lower than the zero-field-cooled one. One of the possible reasons for this difference is flux pinning [49]. The oxygen partial pressure during processing does not affect the general shape of the magnetization curve. However, it makes a difference in the degree of flux pinning.

Several experiments were performed to study the reversibility of the transition of the high-T_c to low-T_c phase;

sample #1: 1%O_2 processing

sample #2: 1%O_2 processing --> 100%O_2 processing

sample #3: 100%O_2 processing

sample #4: 100%O_2 processing --> 1%O_2 processing

Samples #1, #2, and #4 have a high T_c, but sample #3 exhibits a low T_c. It is believed that once a stable cation-site-ordered state is achieved, it is extremely difficult to reverse the system into a metastable cation-site-disordered state.

Fig. 20 shows the inverse susceptibility versus temperature curve for the 1%O_2-processed $Nd_{0.6}Pr_{0.4}Ba_2Cu_3O_{7-\delta}$. From the figure it can be seen that the extension line of the χ^{-1} vs T graph intersects the positive side of the χ^{-1} axis, which means the material is antiferromagnetic. Similar results were found in the $Nd_{0.5}Pr_{0.5}Ba_2Cu_3O_{7-\delta}$ sample.

On T_c-depression model

Fig. 21 shows the T_c-depression curve with increasing x in $Nd_{1-x}Pr_xBa_2Cu_3O_{7-\delta}$. T_c was determined from the intersection point of the zero-diamagnetic moment line and the extension of the tangent of greatest slope to the zero-field-cooled magnetization. The T_c of

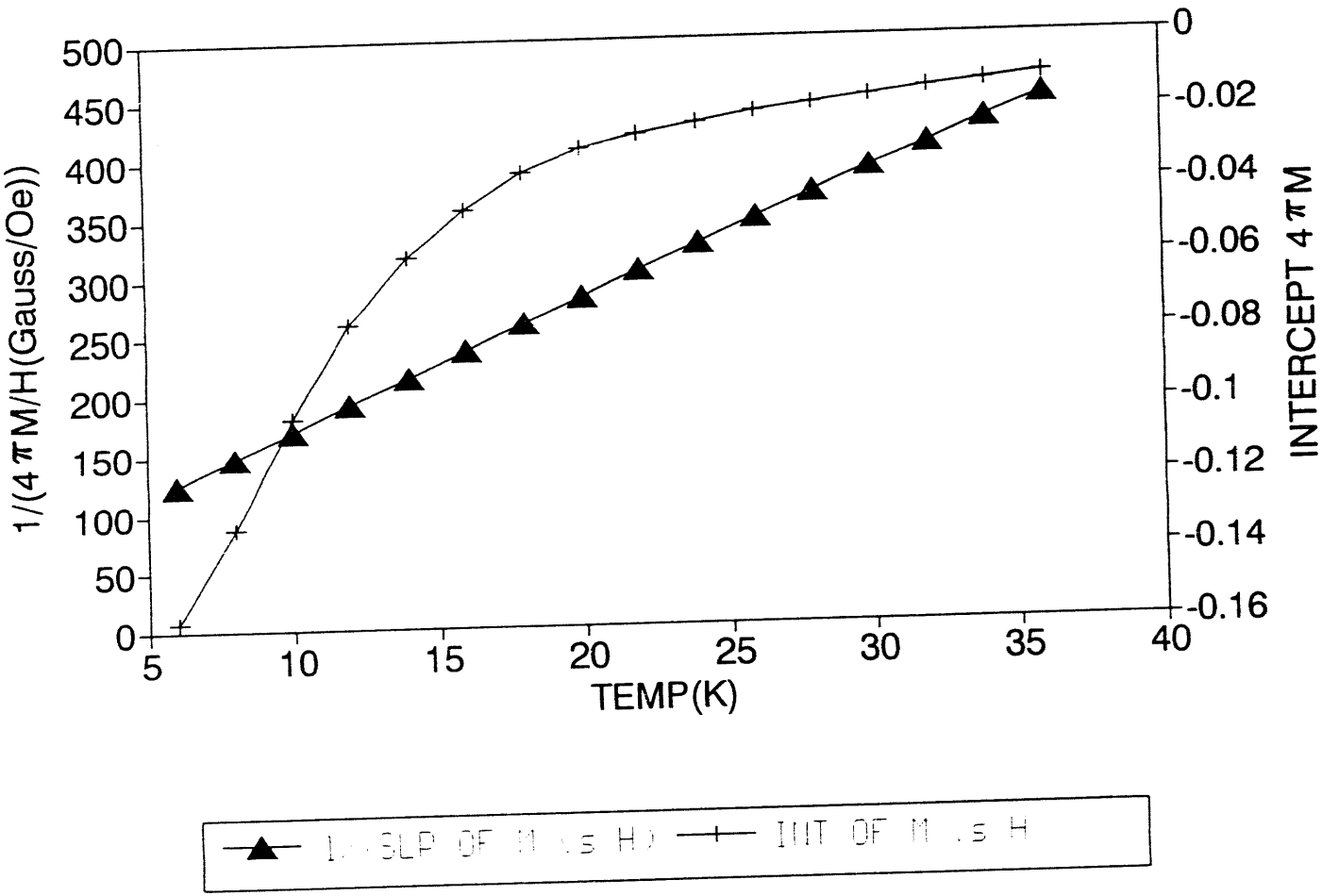

Figure 20 Inverse susceptibility vs temperature graph of $1\%O_2$-processed $Nd_{0.6}Pr_{0.4}Ba_2Cu_3O_{7-\delta}$

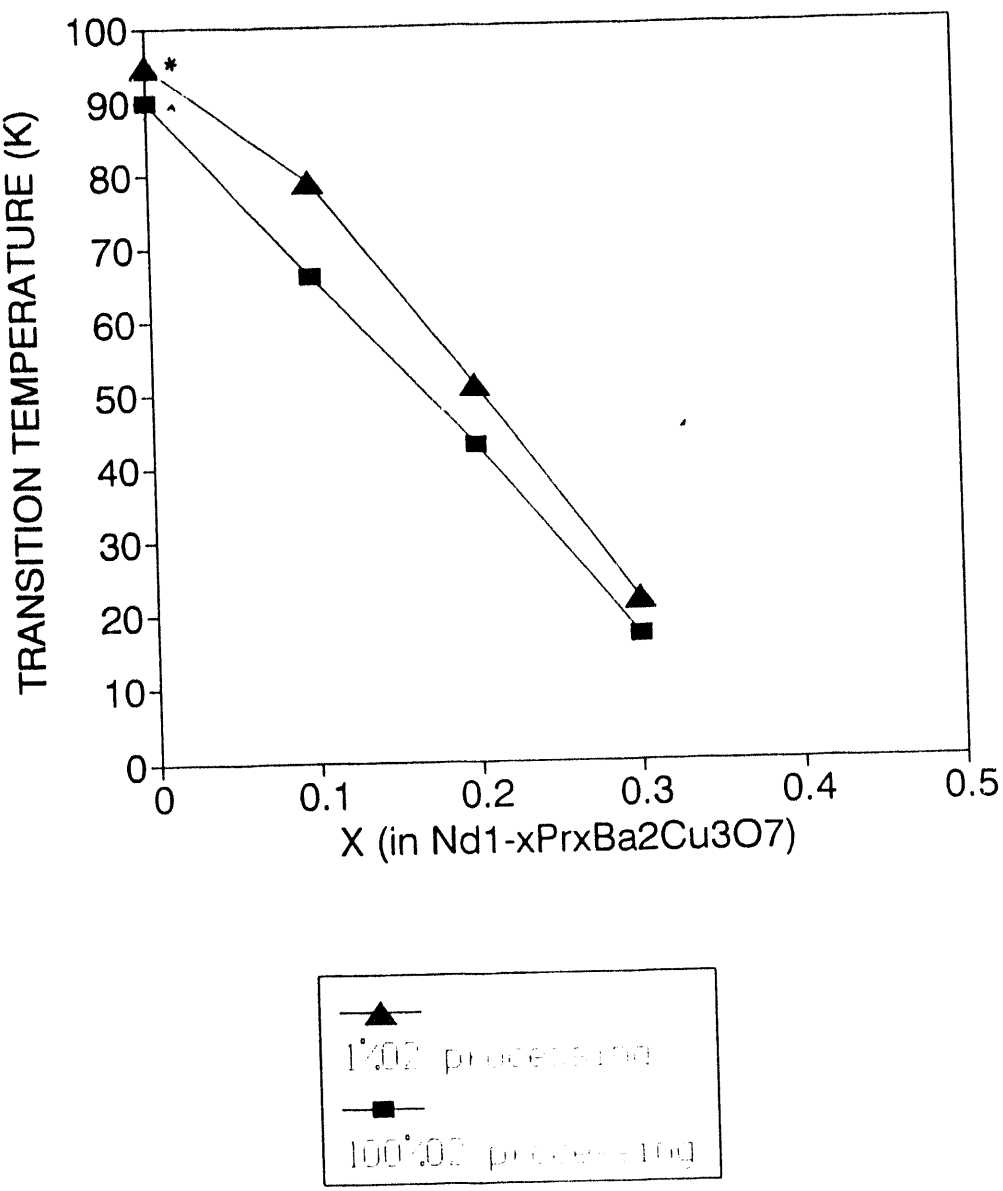

Figure 21 T_c-depression curve (*ref. 54, ^ref. 59}

both the $1\%O_2$ and the $100\%O_2$ processed samples were determined. The sample with $x=0.4$ does not show a superconducting transition at all. Therefore, it can be concluded that superconductivity in $Nd_{1-x}Pr_xBa_2Cu_3O_{7-\delta}$ disappears between $x=0.3$ and $x=0.4$. These results agree well with data of other researchers [29-31]. Models have been proposed to explain the depression of Tc in the RE-Pr-Ba-Cu-O system [11,50-52]. Most of these models are based on experimental results such as those shown in Fig. 21. Since the shape of the T_c-depression curve can be drastically changed by employing different processing parameters, both the employed processing method and concomitant structural change should be considered in order to develop a new model.

According to Gupta and Gupta [24], and Veal [25], the existence of four-fold planar coordinated (FFPC) Cu in the chain-sites is an essential feature for superconductivity. Using a chemical valence model, Veal et al. showed that the number of holes created in the conduction band depends on the configuration of oxygen defects on the basal plane. They also correlated the relationship between hole concentration and Tc. As can be seen from Fig. 22, three kinds of sites on the basal plane can be considered. An oxygen ion entering site-1 does not affect the charge transfer since charge neutrality is maintained locally. The occupation of an O^{2-} ion on this site robs one electron from each Cu ion, which converts the valence of two Cu's from +1 to +2. No electrons have to be transported from outside the basal plane. If the oxygen ion is added to site-2, only one of the Cu ions can give up its electron to an oxygen ion since the other Cu ion has already lost its electron to its neighbor. In this case, one electron should be relocated from elsewhere to satisfy local charge balance. By doing so, one hole is produced in the conduction plane. When site-3 accommodates one oxygen ion, two electrons have to be transferred from other places, creating two holes in the conduction band. Therefore, maximum charge transfer can be attained by maintaining FFPC Cu geometry. In this model, the assumption

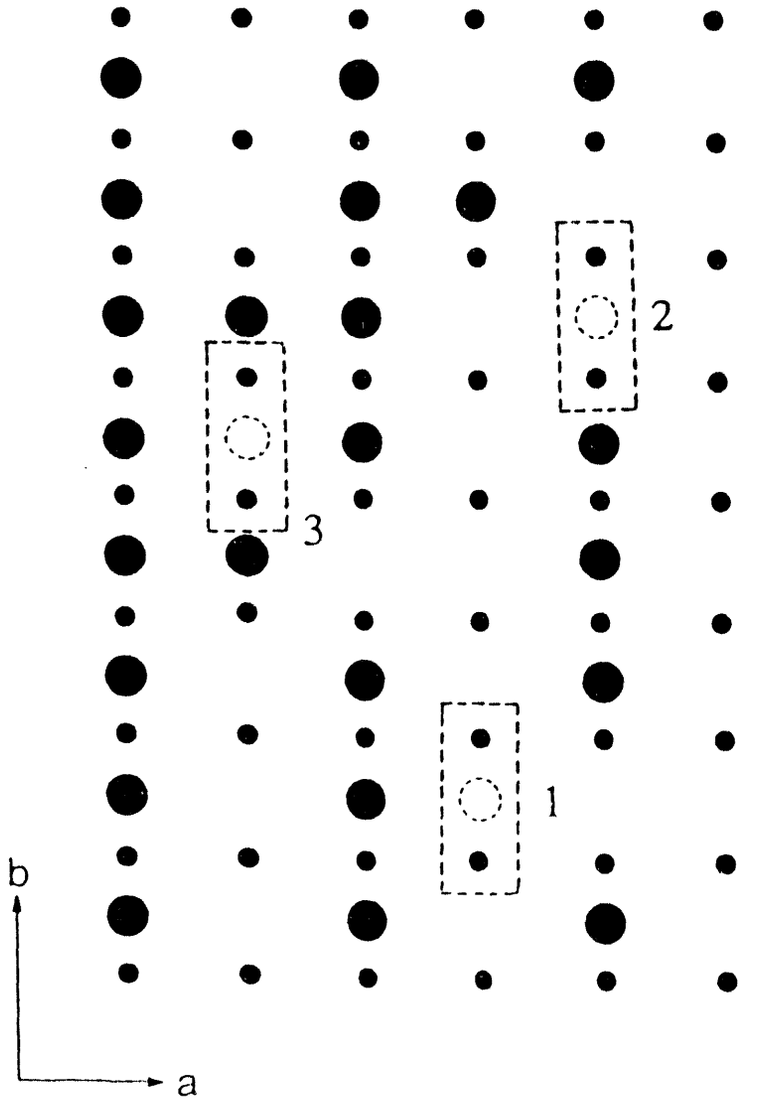

Figure 22 Veal's model illustrating that FFPC Cu insures maximum charge transfer (From ref. 25)

was made that the valence of Cu which is two-fold or either three or four-fold coordinated with oxygen ions are +1 and +2, respectively. From the results of their electronic structure calculations, Gupta et al. showed that charge transfer between planes is intimately related to the geometry of Cu(1) ions in the chain sites. They argued that two-fold, three-fold, and four-fold non-square coordinated Cu configurations are not favored for the creation of holes. Therefore, FFPC Cu ensures that a maximum charge transfer occurs from the charge reservoir to the conduction plane. Any disruption of FFPC Cu hinders the charge transfer, thus degrading superconductivity. However, these models do not pay attention to the fact that the configuration of oxygen defects on the basal plane can be altered significantly by modifying the local environment; especially the two Ba sites with a basal plane in between.

The ionic size of lighter rare-earth elements (LREE) are close to that of Ba, permitting RE ions to occupy Ba sites. The accommodation of $LREE^{3+}$ ions on the Ba^{2+} sites induce oxygen take-up to occur in order to satisfy charge neutrality. Neutron diffraction studies revealed that the total oxygen content and O(5) site occupancy increase as x increases in $Nd_{1+x}Ba_{2-x}Cu_3O_{7+\delta}$ [53]. The depression of T_c with increasing x can be explained by a hole-filling and charge-transfer model [53]. It was pointed out that the geometry of FFPC Cu is affected by the way the extra LREE ions enter the Ba sites. In this case, two extreme conditions can be considered; random and paired occupation of LREE on the Ba sites, which is described in Fig. 23. Neutron diffraction studies revealed that as x extra LREE ions enter Ba sites in a random way, the O(5) sites are occupied by x oxygens while O(1) site occupancy is decreased by 0.5x, where x is in $LREE_{1+x}Ba_{2-x}Cu_3O_{7+\delta}$. Since two LREE ions require one oxygen ion to satisfy charge balance, half of these oxygens are relocated from the O(1) chain-sites and the other half are incorporated from the atmosphere. In Fig. 23, if two LREE ions occupy the Ba sites (site-1 and -2) in a

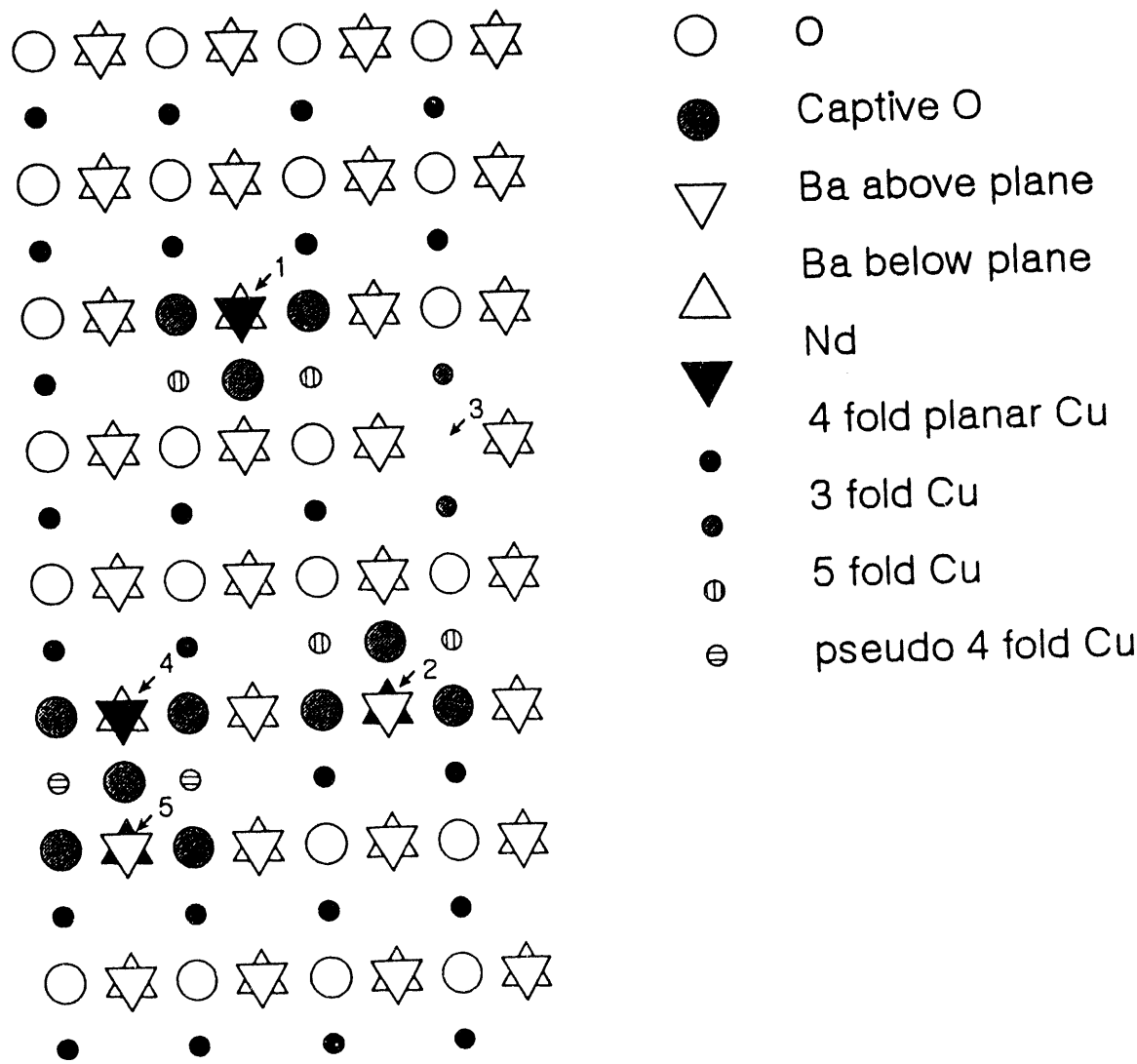

Figure 23 The dependence of charge transfer on the cation distribution (From ref. 53)

random fashion, one oxygen should be added to an anti-chain site in site-2 from the outside, and the other oxygen is relocated from a chain-site somewhere in the structure (site-3). This rearrangement results in the destruction of the FFPC Cu configuration in the chain-site. On the other hand, if two LREE's occupy the Ba sites in a paired way with a O(5) site in-between (site-4 and -5) , charge neutrality can be maintained by accommodating one oxygen ion on the O(5) site without relocating oxygen from the O(1) site. Note that the two paired LREE ions do not have to be located exactly at the same vertical axis since one oxygen can be shared by two adjacent LREE ion neighbors. Therefore, the FFPC Cu structure can be preserved by paired occupation of LREE's on the Ba sites. Since no oxygen remains at the chain sites at high temperature, random occupation of RE ions on Ba sites requires more oxygen than paired occupation does. Therefore, processing a material at low PO_2 forces the extra LREE to occupy Ba sites in a paired fashion [54].

From the phase-equilibria study, it was found that at any PO_2, Ba sites are always occupied by the extra Pr ions in $PrBa_2Cu_3O_{7-\delta}$. It is known that the O(5) site occupancy increases with increasing x in $Y_{1-x}Pr_xBa_2Cu_3O_{7-\delta}$, while the occupation of Nd on the Ba sites can be prevented by a $1\%O_2$ heat-treatment. The addition of Pr ions to $NdBa_2Cu_3O_{7-\delta}$ can be analogous to an increase in x in $Nd_{1+x}Ba_{2-x}Cu_3O_{7+\delta}$. Since the Pr ions on the Ba sites are more effective in destroying superconductivity than the Nd ions on the Ba sites, one of the possible reasons for why the Pr-Ba-Cu-O system is not superconducting is believed to be the destruction of FFPC Cu due to the constant occupation of the Pr ions on the Ba sites. The addition of Pr ions to the Nd123 structure always causes disruption of FFPC Cu, destroying superconductivity. Although this effect seems to play a dominant role in this system, other effects should also be considered. As in the other systems, the number of FFPC Cu can be varied by changing the PO_2 during processing. A lower T_c is

produced by a 100%-O_2 heat-treatment, since high PO_2 processing maximizes the number of extra Pr ions on the Ba sites and favors their random occupation. On the other hand, the T_c of the sample was increased by approximately 10K by processing the material at 1%O_2 atmosphere. This is possible due to the combined effect of the minimization of Pr occupancy on the Ba sites and maximization of the paired occupation.

The relationship of processing-structure-properties

The processing-structure-property relationships in $Nd_{1-x}Pr_xBa_2Cu_3O_{7-\delta}$ is recapitulated in Fig. 24.

1. Oxygen partial pressure during the processing affects both the occupancy of the extra Pr ions on the Ba sites, and the distribution of these ions throughout the sample (random or paired fashion).

2. This cation-site ordering affects the distribution of the oxygen defects on the basal plane.

3. The oxygen ordering modifies the coordination of Cu(1) ions in the chain sites.

4. The geometry of the Cu ions affect the number of holes produced in the conduction plane, resulting in a variation of T_c.

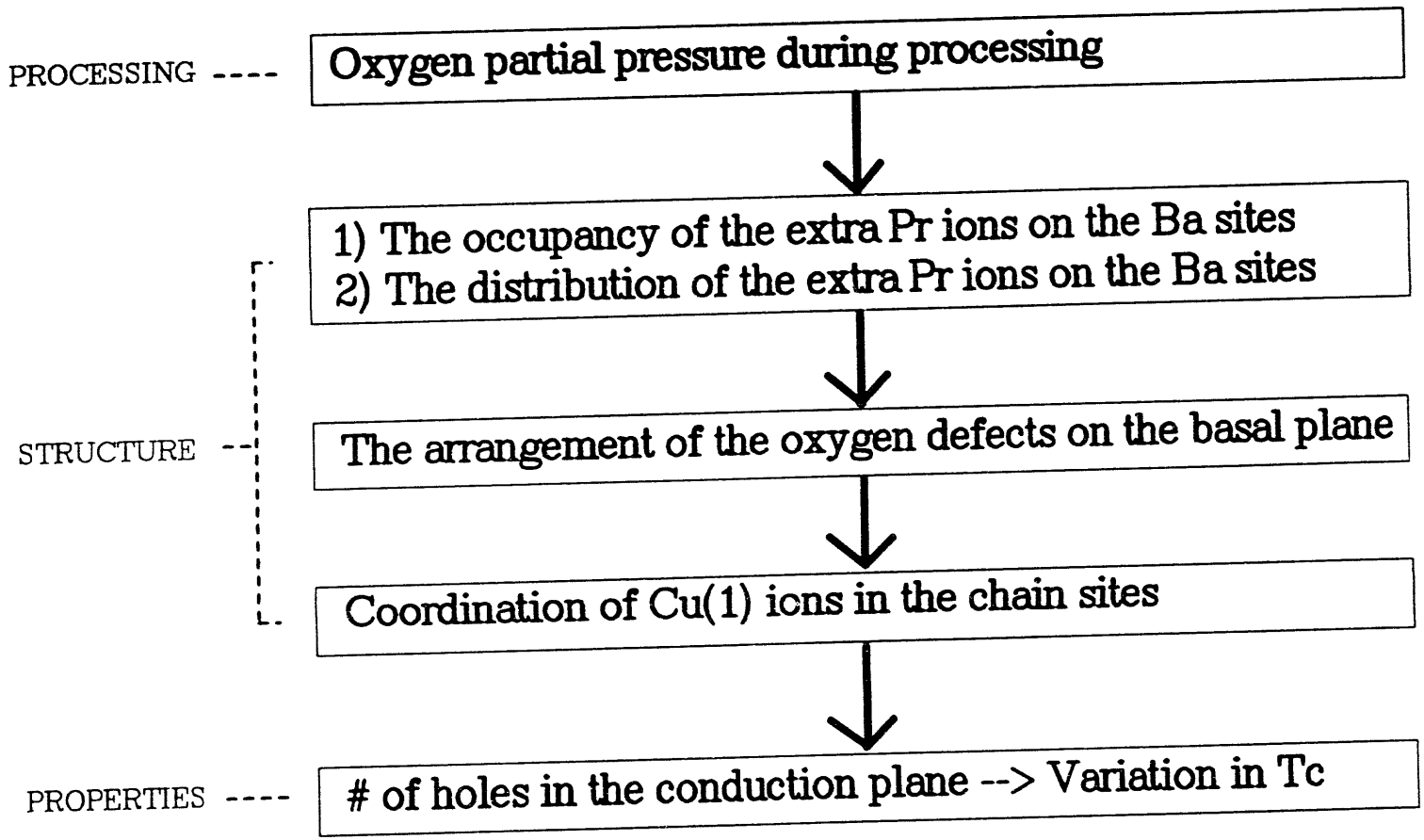

Figure 24 The processing-structure-properties relationship in Nd-Pr-Ba-Cu-O

CONCLUSIONS

The superconducting transition temperature of $Nd_{1-x}Pr_xBa_2Cu_3O_{7-\delta}$ can be varied by employing different oxygen partial pressures during processing. Low PO_2 processing produced a higher value of T_c, which may be produced by the minimization of extra Pr ions on the Ba sites and the maximization of their paired occupancy. Rietveld analysis reveals that structural changes occur anomalously along the c direction in the unit cell. Since this anomalous behavior occurs near the x=0.3-0.4 region where superconductivity disappears, it seems that the structural change in this direction is related to the destruction of superconductivity. This structural change may be produced by a change in the arrangement of cations. Although it is not clear at this stage what exact mechanism governs this structural change, it is plausible to consider that this structural change may play an important role in the destruction of superconductivity. The model developed here suggests that T_c decreases with increasing x in $Nd_{1-x}Pr_xBa_2Cu_3O_{7-\delta}$ because the number of conduction holes are diminished. The decrease in the concentration of conduction hole is believed to be produced by the destruction of FFPC Cu in the chain-sites due to the increase in the number of extra Pr ions on the Ba sites.

GENERAL CONCLUSIONS

1. It was confirmed that at ambient atmosphere Pr123 contains $Pr123_{ss}$ and $BaCuO_2$ as an impurity phase.
2. The amounts of the Pr ions which occupy the Ba sites can be minimized by processing the material at low PO_2 (0.01-0.001 atm)
3. Although the size of the Nd and Pr ions are very similar and they are isovalent, it seems that there is a slight structural difference between Nd-Ba-Cu-O and Pr-Ba-Cu-O.
4. A difference in the way cations are distributed along the [1/2 1/2 1] direction may play an important role in destruction of superconductivity.

Although we could not answer the question of why Pr-Ba-Cu-O is not superconducting conclusively, growing evidence suggest that there is a slight structural difference between superconducting Nd-Ba-Cu-O and non-superconducting Pr-Ba-Cu-O system. Based on the discussion in this thesis, we suggest the following hypothesis;

The Pr-Ba-Cu-O system is not superconducting because of the destruction of FFPC Cu geometry due to the permanent occupation of Pr ions on the Ba sites.

REFERENCES

1 H. K. Onnes, 'Further experiments with liquid helium. C. On the change of electric resistance of pure metals at very low temperatures, etc. 4. The resistance of pure mercury at helium temperatures,' *RN*, **13**, 1274-1276 (1911)

2 J. G. Bednorz and K. A. Muller, Z. Phys. B **64**, 189-193 (1986)

3 M. K. Wu, J. R. Ashburn, C. J. Torng, P. H. Hor, R. L. Meng, L. Gao, Z. J. Huang, Y. Q. Wang and C. W. Chu, Phys. Rev. Lett. **58** (9) 908-10 (1987)

4 T. A. Vanderah et al. eds. *Chemistry of Superconductor Materials*, Noyes Publications, New Jersey (1992).

5 P. H. Hor, R. L. Meng, Y. Q. Wang, L. Gao, Z. J. Huang, J. Bechtold, K. Forster, and C. W. Chu, Phys. Rev. Lett. **58**, 1891 (1987).

6 E. M. Engler, V. Y. Lee, A. I. Nazzal, R. B. Beyers, G. Lim, P. M. Grant, S. S. P. Parkin, M. L. Ramirez, J. E. Vazquez, and R. J. Savoy, J. Am. Chem. Soc.C ommun. **109**, 2848 (1987).

7 J. M. Tarascon, W. R. McKinnon, L. H. Greene, G. W. Hull, and E. M. Vogel, Phys. Rev. B**36**, 226 (1987).

8 K. Zang, Ph.D. thesis, Illinois Institute of Technology, 1988, unpublished.

9 G. Y. Guo, W. M. Temmerman, Phys. Rev. B**41**, 6372 (1990).

10 B. Okai, K. Takahashi, H. Nozaki, M. Saeki, M. Kosuge, and M. Ohta, Jpn. J. Appl. Phys. **26**, L1648 (1987).

11 A. Kebede, C. S. Jee, J. Schwegler, J. E. Crow, T. Mihalisin, G. H. Myer, R. E. Salomon, R. P. Guertin, Phys. Rev. B**40**, 4453 (1989).

12 M. E. Lopez-Morales, D. Rios-Jara, J. Taguena, R. Escudero, S. La Placa, A. Bezinge, V. Y. Lee, E. M. Engler, P. M. Grant, Phys. Rev. B**41**, 6655 (1990).

13 S. K. Malik, C. V. Tomy, Parag Bhargava, Phys. Rev. B**44**, 7042 (1991).

14 H. D. Yang, M. W. Lin, Phys. Rev. B**44**, 5384 (1991).

15 S. K. Malik, S. M. Pattalwar, C. V. Tomy, Ram Prasad, N. C. Soni, K. Adhikari, Phys. Rev. B**46**, 524 (1992).

16 H. D. Yang, M. W. Lin, C. K. Chiou, Phys. Rev. B**46**, 1176 (1992).

17 H. B. Radousky, A review of the superconducting and normal state properties of $Y_{1-x}Pr_xBa_2Cu_3O_7$, J. Mater. Res. **7** (1992).

18 J. Fink, N. Nuecker, H. Romberg, M. Alexander, M. B. Maple, J. J. Neumeier, J. W. Allen, Phys. Rev. B**42**, 4823 (1990).

19 D. P. Norton, D. H. Lowndes, B. C. Sales, J. D. Budai, B. C. Chakoumakos, H. R. Kerchner, Phys. Rev. Lett. **66**, 1537 (1991).

20 D. M. Deleeuw, C. A. H. A. Mutsaers, H. A. M. Van Hal, H. Verweij, A. H. Carim, and H. C. A. Smoorenburg, Physica C**156**, 126 (1988).

21 T. J. Folkerts, K. W. Dennis, S. I. Yoo, Y. Xu, M. J. Kramer, R. W. McCallum, "Recrystallization of Amorphous and Nonocrystalline $NdBa_2Cu_3O_{7-x}$ and $GdBa_2Cu_3O_{7-x}$", IEEE Transanctions on Applied Superconductivity (in press).

22 J. D. Jorgensen, D. G. Hinks, B. A. Hunter, R. L. Hitterman, A. W. Mitchell, P. G. Radaelli, B. Dabrowski, J. L. Wagner, H. Takahashi, E. C. Larson, submitted to *Lattice Effects in High Tc Superconductors*, Y. Bar-Yam, T. Egami, J.Mustre-de Leon, A. Bishop, eds., (World Scientific Publ.,Singapore) to be published.

23 J. D. Jorgensen, D. G. Hinks, P. G. Radaelli, Shiyou Pei, P. Lightfoot, B. Dabrowski, C. U. Segre, B. A. Hunter, *M2S-HTSC3:Proceedings of the third International Conference on Materials and Mechanism of Superconductivity High-Temperature Superconductors*, Kanazawa, Japan, July 22-26, 1991.

24 M. Gupta and R. P. Gupta, Physica C **185-189**, 851 (1991)

25 B. W. Veal and A.P.Paulikas, Physica C **184**, 321 (1991)

26 P. Karen, H. Fjellvag, O. Braaten, A. Kjekshus, H. Bratsberg, Acta Chemi. Scand. **44**, 994-1001 (1990).

27 S. A. Hodorowicz, J. Czerwonka, H. A. Eick, J. Solid State Chem. **88**, 391-400 (1990).

28 J. J. Neumeier, T. Bjornholm, M. B. Maple, J. J. Rhyne, J. A. Gotaas, Physica C**166**, 191 (1990).

29 H. Iwasaki, J-I. Sugawara, N. Kobayashi, Physica C **185-189**, 1249-1250 (1991).

30 K. Koyama, Y. Suzuki, S. Noguchi, Jpn. J. Appl. Phys. **27**, 1862-1866 (1988).

31 H. Jhans, S. K. Malik, S. K. Dhar, R. Vijayaraghavan, Physica C **207**, 247-254 (1993).

32 K. No, J. D. Verhoeven, R. W. McCallum, E. D. Gibson, *Proc.Appl.Superconductivity Conf.* (San Fransisco,CA,1988).

33 J. E. Ullman, R. W. McCallum, J. D. Verhoeven, J. Mater. Res. **4**, 752 (1989).

34 Larson & Von Dreele, GASA program software (1988)

35 K. Kinoshita, A. Matsuda, H. Shibata, T. Ishii, T. Watanabe, T. Yamada, Jpn. J. Appl. Phys. **27**, 11642 (1988)

36 B. Okai, M. Kosuge, H. Nozaki, K. Takahashi, M. Ohta, Jpn. J. Appl. Phys. **27**, L41 (1988)

37 R. S. Roth, K. L. Davis, J. R. Dennis, Adv. Ceram. Mater.,2 [**313**] 303-312 (1987)

38 H. Migeon et al., Rev. Chim. Miner., **13**, 440 (1976)

39 M. Arjomand, D. J. Machin, J. Chem. Soc. Dalton Tranc., **11**, 1061-1066 (1975)

40 L. M. Lopata, Ceramurgia Int., **2**, 18 (1976)

41 N. Rosov, J. W. Lynn, Q. Lin, G. Gao, J. W. O'Reilly, P. Pernambuco-Wise, J. E. Crow, Phys. Rev. B**45**, 982 (1992)

42 D. E. Cox, A. I. Goldman, M. A. Subramanian, J. Gopalakrishnan, A. W. Sleight, Phys. Rev. B**40**, 6998 (1989)

43 T. Aselage, K. Keefer, J. Mater. Res. **3**, 1279 (1988)

44 T. Wada, N. Suzuki, T. Maeda, A. Maeda, S. Uchida, K. Uchinokura, S. Tanaka, Appl. Phys. Lett. **52**, 23 (1988)

45 S. K. Malik, S. M. Pattalwar, C. V. Tomy, Ram Prasad, N. C. Soni, K. Adhikury, Phys. Rev. B**46**, 524 (1992)

46 "The Rietveld Method" ed. by R.A.Young, Oxford Univ. Press (1993)

47 H. M. Rietveld, Acta Crystallogr., **22**, 151-2 (1967)

48 H. M. Rietveld, J.Appl. Crystallogr.,**2**, 65-71 (1969)

49 A. P. Malozemoff 'Macroscopic Magnetic Properties of High Temperature Superconductors'

50 E. Orgaz, E. Ruiz-Trejo, Physica C, **194**, 76-80 (1992)

51 Y. Xu, W. Guan, Physica C, **183**, 105-11 (1991)

52 Y. Xu, W. Guan, Phys. Rev.B, **145**, 3176 (1992)

53 M. J. Kramer, S. I. Yoo, R. W. McCallum, W. B. Yelon, H. Xie, P. Allenspach, Physica C **219** 145-155 (1994)

54 M. J. Kramer, A. Karion, K. W. Dennis, M. Park, and R. W. McCallum, J. Elec. Mat. (to appear)

55 B. T. Ahn, V. Y. Lee, R. Beyers, T. M. Gur, and R. A. Huggins, Physica C **167** 529-537 (1990)

56 S. I. Yoo, Ph.D Thesis, Iowa State University, Ames, IA, U. S. A.

57 D. E. Morris, A. G. Markelz, B. Fayn, and J. H. Nickel, Physica C **168**,153 (1990)

ACKNOWLEDGMENTS

First of all, I give thanks to 'God' for giving me a chance to study in the United States of America.

I wish to thank my major professor, Dr. R. W. McCallum, for giving me an opportunity and financial support to explore this 'fascinating world' of superconductivity. I again thank him for his being a 'beacon' throughout this 'expedition'.

I thank my other committee members, Dr. K. Constant, S. Martin, A. Goldman for sincere advice. I also want to thank Dr. M.J.Kramer for his showing me a way to the 'realm' of Rietveld refinement analysis. Special thanks to Mr. K. W. Dennis for his assistance in the performance of this research. I thank many faculty members for providing me with a plethora of 'food for thought' on Materials Science. I also thank Dr. V. G. Young for XRD analysis.

I would like to thank many friends, S. Arrasmith, D. Branagan, T. Bloomer, T. Folkerts, S. Haines, S. Han, Y. Han, J. Lee, L. Margulies, B. Merkle, J. Shield, H. Wu, M. Xu, Y. Xu, S. Yoo, ... , for numerous discussions. I finally want to thank my parents at home for supporting my study abroad.

Without their help, this 'journey' would not have been possible.

This work was preformed at Ames Laboratory, and was supported by the Director of Energy Research, U.S.Department of Energy under contract No. W-7405-ENG-82. The U. S. government has assigned the DOE report number IS-T-1707 to this thesis.

EPILOGUE

Throughout this QUEST, I produced more QUESTIONS than ANSWERS.

DATE
FILMED
7/21/94
END